

University of Groningen

A nexus of intrinsic dynamics underlies translocase priming

Krishnamurthy, Srinath; Eleftheriadis, Nikolaos; Karathanou, Konstantina; Smit, Jochem H.; Portaliou, Athina G.; Chatzi, Katerina E.; Karamanou, Spyridoula; Bondar, Ana Nicoleta; Gouridis, Giorgos; Economou, Anastassios

Published in:
Structure

DOI:
[10.1016/j.str.2021.03.015](https://doi.org/10.1016/j.str.2021.03.015)

IMPORTANT NOTE: You are advised to consult the publisher's version (publisher's PDF) if you wish to cite from it. Please check the document version below.

Document Version
Publisher's PDF, also known as Version of record

Publication date:
2021

[Link to publication in University of Groningen/UMCG research database](#)

Citation for published version (APA):

Krishnamurthy, S., Eleftheriadis, N., Karathanou, K., Smit, J. H., Portaliou, A. G., Chatzi, K. E., Karamanou, S., Bondar, A. N., Gouridis, G., & Economou, A. (2021). A nexus of intrinsic dynamics underlies translocase priming. *Structure*, 29(8), 846-858.e7. <https://doi.org/10.1016/j.str.2021.03.015>

Copyright

Other than for strictly personal use, it is not permitted to download or to forward/distribute the text or part of it without the consent of the author(s) and/or copyright holder(s), unless the work is under an open content license (like Creative Commons).

The publication may also be distributed here under the terms of Article 25fa of the Dutch Copyright Act, indicated by the "Taverne" license. More information can be found on the University of Groningen website: <https://www.rug.nl/library/open-access/self-archiving-pure/taverne-amendment>.

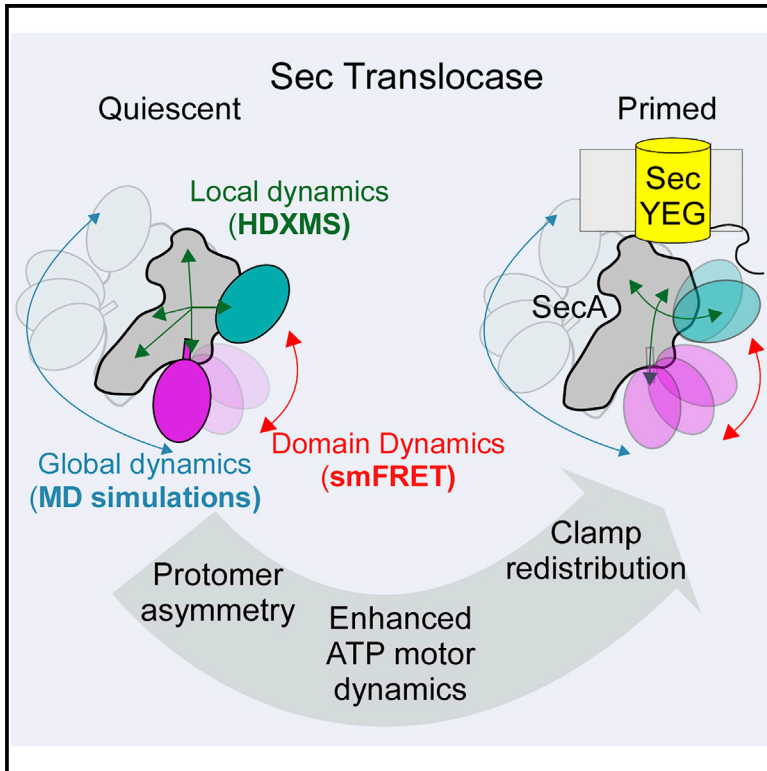
Take-down policy

If you believe that this document breaches copyright please contact us providing details, and we will remove access to the work immediately and investigate your claim.

Downloaded from the University of Groningen/UMCG research database (Pure): <http://www.rug.nl/research/portal>. For technical reasons the number of authors shown on this cover page is limited to 10 maximum.

A nexus of intrinsic dynamics underlies translocase priming

Graphical abstract



Authors

Srinath Krishnamurthy,
Nikolaos Eleftheriadis,
Konstantina Karathanou, ...,
Ana-Nicoleta Bondar,
Giorgos Gouridis,
Anastassios Economou

Correspondence

g.gouridis@imbb.forth.gr (G.G.),
tassos.economou@kuleuven.be (A.E.)

In brief

Krishnamurthy et al. dissect the bacterial Sec preprotein translocase using a combination of biophysical tools and reveal a nexus of multi-level intrinsic dynamics that regulates its activity and function. These data reveal the structural dynamics basis of translocase priming for high-affinity binding of multiple clients and ADP release.

Highlights

- SecA exhibits global, domain, and local intrinsic dynamics that control its activity
- Cognate ligands alter dynamics nexuses to regulate dynamics and function
- SecYEG channel binding catalytically primes SecA by increasing ATP motor dynamics
- Channel binding redistributes the preprotein client binding clamp



Article

A nexus of intrinsic dynamics underlies translocase priming

Srinath Krishnamurthy,^{1,5} Nikolaos Eleftheriadis,^{1,5} Konstantina Karathanou,² Jochem H. Smit,¹ Athina G. Portaliou,¹ Katerina E. Chatzi,¹ Spyridoula Karamanou,¹ Ana-Nicoleta Bondar,² Giorgos Gouridis,^{1,3,4,*} and Anastassios Economou^{1,6,*}

¹KU Leuven, University of Leuven, Rega Institute, Department of Microbiology and Immunology, 3000 Leuven, Belgium

²Freie Universität Berlin, Department of Physics, Theoretical Molecular Biophysics Group, Arnimallee 14, 14195 Berlin, Germany

³Molecular Microscopy Research Group, Zernike Institute for Advanced Materials, University of Groningen, Nijenborgh 4, 9747 AG Groningen, the Netherlands

⁴Structural Biology Division, Institute of Molecular Biology and Biotechnology (IMBB-FORTH), Nikolaou Plastira 100, Heraklion-Crete, Greece

⁵These authors contributed equally

⁶Lead contact

*Correspondence: g.gouridis@imbb.forth.gr (G.G.), tassos.economou@kuleuven.be (A.E.)

<https://doi.org/10.1016/j.str.2021.03.015>

SUMMARY

The cytoplasmic ATPase SecA and the membrane-embedded SecYEG channel assemble to form the Sec translocase. How this interaction primes and catalytically activates the translocase remains unclear. We show that priming exploits a nexus of intrinsic dynamics in SecA. Using atomistic simulations, smFRET, and HDX-MS, we reveal multiple dynamic islands that cross-talk with domain and quaternary motions. These dynamic elements are functionally important and conserved. Central to the nexus is a slender stem through which rotation of the preprotein clamp of SecA is biased by ATPase domain motions between open and closed clamping states. An H-bonded framework covering most of SecA enables multi-tier dynamics and conformational alterations with minimal energy input. As a result, cognate ligands select preexisting conformations and alter local dynamics to regulate catalytic activity and clamp motions. These events prime the translocase for high-affinity reception of non-folded preprotein clients. Dynamics nexuses are likely universal and essential in multi-liganded proteins.

INTRODUCTION

Protein machines handle replication, transcription, and unwinding of nucleic acids or folding, disaggregation, degradation, and secretion of polypeptides (Avellaneda et al., 2017; Flechsig and Mikhailov, 2019; Kurakin, 2006). Such machines are commonly autoinhibited and become activated by their partner subunits and polymeric substrates and then spend energy to remodel the latter. Their function exploits intrinsic dynamics that span multiple time regimes (Henzler-Wildman et al., 2007; Yang et al., 2014).

Unique to each protein, dynamics describe combined relative motions of protomers/subunits (hereafter “quaternary”), tertiary motions within a single chain (“global”), and relative “domain” and “local” motions (e.g., loss or displacement of secondary structure elements, hinges, or loops, and fluctuations of interactions between amino acids). Intrinsic dynamics usually underlie allosteric interactions; however, their regulation or coupling to function remains unclear (Bhabha et al., 2015; Loutchko and Flechsig, 2020; Zhang et al., 2020).

Here, we studied the four-domain DEAD box helicase member SecA, which chaperones and translocates bacterial secretory

polypeptides. SecA binds to the SecYEG channel in membranes to form the primed Sec translocase allosteric ensemble (Ahdash et al., 2019; Corey et al., 2019; Gouridis et al., 2013) and interacts with non-folded clients bearing signal peptides, nucleotides, lipids, and chaperones and undergoes dimer-to-monomer transitions (De Geyter et al., 2020; Rapoport et al., 2017; Tsirigotaki et al., 2017a). Orderly, sequential ligand interactions transform the translocase from a quiescent to an active state. However, the presumably multi-tier dynamics and energetics and their link to translocation work remain elusive.

SecA, a dimeric, autoinhibited ATPase (Figure 1) (Sianidis et al., 2001; Wowor et al., 2011), retains a tight ADP-stabilized state until it peripherally associates with the channel with one protomer, to form the primed translocase. This converts SecA to a 10-fold tighter preprotein binder (Figure 1) (Gouridis et al., 2013) and somehow prepares it for ATP hydrolysis turnover once a signal peptide and the mature domain bind (Fak et al., 2004; Gouridis et al., 2009; Sianidis et al., 2001). SecA then converts to a monomeric processive motor working through mechanical strokes, Brownian ratcheting, and/or alternating channel conformations (Allen et al., 2016; Catipovic et al., 2019; Economou and Wickner, 1994; Vandenberk et al., 2019).



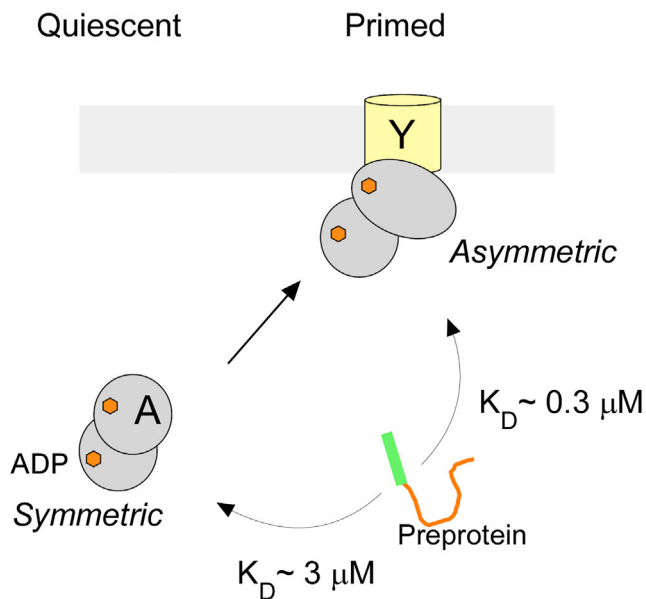


Figure 1. Priming of the Sec translocase

Cytoplasmic SecA is a catalytically quiescent symmetric dimer that binds the SecYEG channel asymmetrically and forms the primed translocase holoenzyme. Primed SecA₂ has 10-fold higher preprotein affinity compared with quiescent SecA₂. Orange hexagon, ADP.

SecA's helicase motor (nucleotide binding domains [NBD] 1 and 2) is fused to an ATPase-suppressing C domain and a pre-protein binding domain (PBD) (Figures 2A, S1A, S1B, and S1C, I). PBD, rooted via a stem in NBD1, intrinsically rotates toward NBD2 to clamp mature domains (Bauer and Rapoport, 2009) and occupies three distinct states: wide open, open, and closed (Figure 2A; Table S1, II, III) (Ernst et al., 2018; Sardis and Economou, 2010; Vandenberg et al., 2019). Moreover, the PBD carries both the signal peptide cleft in its “bulb” globular domain and the mature domain binding site on the narrow stem that connects it to NBD1 (Chatzi et al., 2017) (Figures 2A, S1B, and S1C, II). When the PBD is in the wide-open state, the dynamic C tail of SecA folds over the signal peptide cleft and stem regions, where it binds as a pseudo-substrate guarding access to the client binding surfaces (Chatzi et al., 2017; Gelis et al., 2007).

Structures of soluble and detergent-solubilized channel/pre-protein SecA states revealed their static architectures (Ma et al., 2019; Rapoport et al., 2017; Sardis and Economou, 2010), but how the underlying dynamics prime (channel binding) and activate (channel and preprotein binding) the translocase in a physiological membrane environment remains elusive. Here, we determined the intrinsic dynamics of SecA and probed how they underlie the conversion from quiescence to priming by assembly with the channel, using an integrated approach.

Fully atomistic molecular dynamics (MD) simulations and graph analysis determined global dynamics and H-bond networks that interconnect remote regions of SecA (Karathanou and Bondar, 2019). Single-molecule Förster resonance energy transfer (smFRET) reported on domain dynamics (Gouridis et al., 2015; Kapanidis et al., 2004; Vandenberg et al., 2019), and hydrogen-deuterium exchange mass spectrometry (HDX-MS) identified local dynamics (Tsirigotaki et al., 2017b; Vadas

and Burke, 2015). In both cases translocation-permitting physiological membranes and concentrations under detergent-free conditions were used.

We revealed that SecA comprises an extensive H-bond network that yields a nexus of multi-level intertwined dynamics that combine quaternary effects from dimerization, including dimer-to-monomer transitions; global and domain effects in each protomer; and multiple islands of local intrinsic dynamics. Within each protomer, specific islands in the helicase motor, its associated scaffold helix, and the stem conformationally cross-talk and affect the interconversions of the preprotein clamp between three states. ADP that occupies preactivated SecA tightly restricts these local dynamics but does not affect clamp motions. Dimeric, cytoplasmically diffusing SecA maintains a predominantly wide-open clamp with weak client access. In contrast, the channel, on one hand, binds to dimeric SecA and, on the other, uses its carboxy-terminal region to trigger redistribution of the SecA clamp equally between the three states in the channel-bound active protomer. This structural transformation allows increased access to preprotein clients and enhanced flexibility due to the relief of ADP-driven suppression of SecA local dynamics. These events thereby prepare the translocase for pre-protein-mediated ADP release and activation of the enzyme for secretion work. Our data reveal how multiple ligands of a protein machine can promote stepwise priming, activation, and catalysis by exploiting sophisticated and coordinated multi-level intrinsic dynamics. The tools used here will be widely available in other membrane-embedded systems.

RESULTS

Cytoplasmic SecA₂ has restricted domain motions and a wide-open clamp

To understand how the cytoplasmic SecA₂ is autoinhibited but becomes primed and activated when channel-bound, we first probed its global dynamics using simulations in bulk water. Two different, likely physiological, dimers (Gouridis et al., 2013) (Table S2), both with their clamps in wide-open states (Figures 2B and S2A), were used as starting structures for two independent simulations.

All four SecA domains, particularly NBD1, are extensively H bonded (Figure S2B) and exhibit similar dynamics irrespective of the protomer to which they belong. Several residues participate in multiple H bonds and/or are hubs in multi-residue H-bond pathways (Figures S2B–S2D; Table S2). During 260 ns MD simulations, both SecA₂ structures displayed only minor domain motions in each of their protomers without loss of the wide-open state (Figures 2B and S2E). The wide-open state is stabilized through multiple interactions that the PBD makes with the wing domain and the C tail. This partially restricts access to the signal peptide cleft (Figure S1C, II–III, top; Table S2).

To monitor domain motions specifically in the clamp we used our established smFRET pipeline (Figures 2C and 2D and S3A) (Vandenberg et al., 2019). His-SecAD2, a single-cysteinyll-pair (V280C_{PBD}/L464C_{NBD2}) derivative, was stochastically labeled with donor and acceptor fluorophores (Vandenberg et al., 2019). The donor of the labeled samples was excited by a laser at an intensity of 0.5 μW and a constant wavelength of 532 nm. All acceptor fluorophore emissions recorded are thus a result

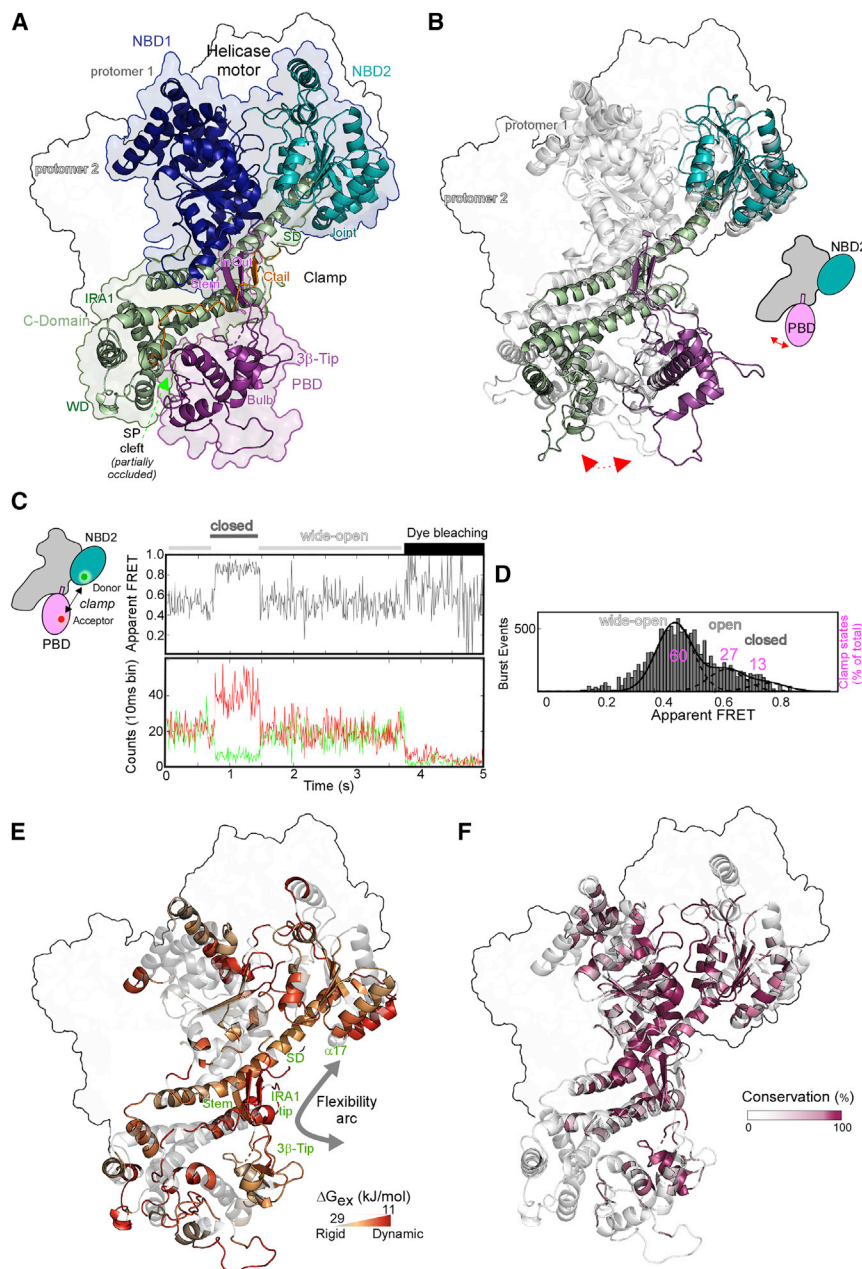


Figure 2. Local dynamics islands in SecA regulate clamp domain dynamics

(A) Domain organization of *ecSecA₂*, modeled after the *B. subtilis* PDB:1M6N in ribbon (shaded surface). The ATPase motor (NBD1 and NBD2, nucleotide binding domains), PBD (preprotein binding domain), and C domain (comprising scaffold [SD], wing [WD], IRA1 [intramolecular regulator of ATPase 1] and C tail) are shown. See also Figure S1.

(B) MD simulation of *ecSecA_{2-1M6N}*. Two coordinate snapshots shown from start (0 ns; gray) and end (262 ns) aligned on their NBD1 (protomer 1: colored as in Figure 2A, protomer 2: contoured).

(C and D) smFRET analysis of PBD motions using His-SecAD2, stochastically labeled with Alexa 555 and Alexa 647, which was either immobilized on a PEG-biotinylated- α -His antibody surface (C) or freely diffusing (50–100 pM) (D). Cold His-SecAD2 (1 μ M) promoted dimers (see Figure S3A). (C) Top: representative FRET trace (1 of 162) showing rare transitions between the indicated states. Bottom: photon counts collected during FRET trace recording. (D) The FRET value of every labeled SecA molecule randomly diffusing through the confocal volume (i.e., burst event, y axis, left) was calculated (apparent FRET, E^* , x axis) and plotted. Derived histograms (>10,000 total burst events binned in E^* tranches; y axis, right) were fitted to a minimum of three Gaussians (Figure S3B) representing distinct quantified clamp states (as indicated). Sum of three integrals = 100%; each state is a percentage of the total. $n = 6$.

(E) ΔG_{ex} values (in kJ/mol) were calculated by PyHDX (Smit et al., 2020) from HDX-MS experiments and visualized on the dimeric *ecSecA_{2-1M6N}* apo-protein structure. Residues are colored on a linear scale from gray (29 kJ/mol, rigid) to red (11 kJ/mol, dynamic). Highly rigid residues ($\Delta G_{ex} > 29$ kJ/mol) are in transparent gray (see also Figure S4; Table S3).

(F) Highly conserved residues in 200 SecAs, derived from ConSurf (Ben Chorin et al., 2020), colored as indicated onto *ecSecA_{2-1M6N}* (represented as in [A]).

of FRET from donor emission. In the event of donor fluorophore bleaching, acceptor emissions are also simultaneously lost, as is the case in most of our traces. The FRET state of labeled His-SecAD2 reports directly on how proximal PBD and NBD2 are and, thus, on clamp motions (Figure 2C, cartoon). Heterodimers of His-SecAD2 were generated by mixing fluorescent kinetic monomers with excess unlabeled His-SecAD2. FRET traces from surface-immobilized heterodimers were recorded as a function of time on a confocal microscope (Gouridis et al., 2015). The analysis of 162 such trajectories demonstrated that the clamp of SecA₂ predominantly existed in a low FRET state, consistent with the wide-open clamp state, rarely transiting to the open and closed states (~10% of the 162 traces; Figures 2C, S3C, and S3D) (Sardis and Economou, 2010). These data

reveal that the clamp is intrinsically dynamic, with individual states stable, with lifetimes in the near-second time regime, indicative of large domain motions (Henzler-Wildman and Kern, 2007).

Clamp states were quantified by solution smFRET. Fluorescently labeled heterodimers were monitored as they freely diffused through the confocal volume. Following pulsed interleaved excitation (Muller et al., 2005; Vandenberg et al., 2019), >10,000 photon burst events from molecules carrying both fluorophores (which hence could transfer Förster resonance energy) were analyzed per experiment (Figure 2D). Two-dimensional plots of stoichiometry versus apparent FRET efficiency were globally fitted with a mixture model of Gaussians (Figures S3B and S3E) (Gouridis et al., 2019). The data were best fitted with three distributions and quantified using the area under the curve, taking the sum of all states as 100% (Figure 2D). The clamp of SecA predominantly sampled the wide-open state (60% of the population) and less so the open and closed states (27% and

13%, respectively). We calculated accurate FRET distances (Hellenkamp et al., 2018) between the two fluorophores on SecA and derived distances of 61, 46, and 36 Å for the wide-open, open, and closed states, respectively. These previously obtained values (Vandenberk et al., 2019) and distances derived from crystal structures (Table S1V) are all in similar ranges.

Collectively, these data show that SecA₂ displays limited intrinsic domain dynamics and has its clamp predominantly in the wide-open state. This state is maintained by several interprotomer interactions and limits access to the signal peptide cleft (Gelis et al., 2007) (Table S1; Figure S1C, III, top).

Conserved islands of intrinsic dynamics in SecA₂

To define the underlying residue dynamics that define domain motions, we determined the residue-level local dynamics of SecA₂ using HDX-MS. This technique non-invasively monitors loss or gain of backbone H bonds, common in secondary structure, at low-micromolar concentrations, near-residue resolution, and a timescale of seconds (Brown and Wilson, 2017; Hu et al., 2013; Skinner et al., 2012).

SecA₂ was diluted to ~2 μM into D₂O buffer for various times. Samples were acid quenched and protease digested (Wowor et al., 2014), and D uptake was determined by mass spectrometry (Figure S4A, I). One hundred ninety peptides with high signal/noise ratio yielded ~95% primary sequence coverage (Table S3). The D uptake for each peptide was expressed as a percentage of its fully deuterated control (taken as 100%). D-uptake data were then processed by our in-house software PyHDX (Smit et al., 2020) to yield Gibbs free energy of exchange (ΔG_{ex} , kJ mol⁻¹) values for each residue. ΔG_{ex} values quantify the degree of dynamics existing within the protein backbone to which they are inversely correlated, i.e., lower and higher ΔG_{ex} values represent lower and higher backbone flexibility, respectively.

SecA₂ has several distributed regions of flexibility that together form islands of high intrinsic dynamics (Figure 2E, orange and red; Figure S4B), some of them sharply delimited against an otherwise “rigid” backdrop (gray). Dynamics islands in the nucleotide binding cleft in the ATPase motor and signal peptide clefts are linked by a chain of intrinsic dynamic residues that form a “flexibility arc” that lines the inner walls of the clamp (Figure 2E; gray arrow). The arc includes the 3β-tip_{PBD}, peripheral loops of the PBD core, the three-stranded anti-parallel β sheet formed by the stem (consisting of two anti-parallel β strands and their flexible linker), and the C tail, the tip of IRA1, the motor-associated scaffold with its kinked middle region that ultimately connects to the joint that includes α17_{NBD2S}.

The nucleotide binding cleft and flexibility arc are highly conserved, while the signal peptide cleft is not (Figure 2F). The local dynamics observed are likely fundamental for SecA function and may underpin large-scale domain motions and coupling to nucleotide cycles and client binding.

Monomeric SecA displays enhanced domain dynamics and a distributed clamp

We next determined how dimerization affects the inherent dynamics of the SecA protomer. MD simulations of monomeric SecA revealed that PBD and NBD2 move toward each other, meet within 150 ns, and form a stably closed clamp until the end of the simulation (325 ns). Concomitantly, C-domain sub-

structures undergo domain motions (Figures 3A and S2E–S2G; Video S1). Clamp closing also exposes the signal peptide cleft (Gelis et al., 2007) (Figure S1C, II and III, bottom; Table S1). Some residues negotiate distances of ~2 nm (Figure S2F). During these motions, PBD loses internal H bonds (Figure S2B). We analyzed two coordinate snapshots of the open and closed clamp, representative conformations based on H-bond networks and centrality measurements (Figures S2C, S2D, and S2H). Multiple interdomain salt bridges and dynamic H-bond clusters (mainly between PBD, scaffold, and NBD2) and an extensive local hydration network lie behind clamp motions (Figures S2I and S2J; Table S2). Initially, the salt bridge of R709_{WD} with E294_{PBD} of a signal peptide cleft loop breaks (Figure S2H, left). Then, the PBD moves toward and binds NBD2 using two prongs to form a closed conformation (prong1, aa 250–275; prong2 or 3β tip, aa 320–347; Figures 3A; S1C, II and III, bottom; S2H, right; and S2J). In this “loosely closed” conformation identified for the first time by these MD simulations, the PBD is more peripherally associated compared with the tightly closed conformation seen in SecYEG:SecA:ADP.BeF₄ crystals (Zimmer et al., 2008).

smFRET experiments were carried out at low protein concentrations (50–100 pM) at which His-SecAD2 existed as kinetic monomers. Analysis of 84 trajectories from surface-immobilized His-SecAD2 demonstrated that the clamp of monomeric SecA freely interconverted between wide-open, open, and closed states (representative trace, Figures 3B, S3C, and S3D), revealed by solution smFRET to be sampled almost equally (29%, 37%, and 34%, respectively) (Figures 3C, lanes 4–6; S3F; and S6A, I–II). Therefore, dimerization is a key extrinsic factor that suppresses the intrinsic clamp motions inherent to the monomer.

SecA monomers display enhanced local dynamics

To monitor the local dynamics of monomeric SecA, we analyzed mSecA, a fully functional derivative with reduced dimerization K_d (~130 μM) (Gouridis et al., 2013), by HDX-MS. We compared mSecA with SecA₂, focusing only on prominent differences within 5 min of D exchange. To ease comparison, D-uptake differences (ΔD) of a control state (Figure 3D, upper left pictogram, top) were compared with a test state (bottom). Positive or negative values indicate regions with enhanced or suppressed dynamics (green/purple, respectively), quantified as minor or major (% ΔD ; 10%–20% light hues; >20% dark hues).

Monomerization increased the dynamics specifically in the nucleotide binding cleft and in the flexibility arc, including most of the scaffold (Figures 3D, green, and S5A, I; Table S3). Most of the destabilized elements corresponded to regions that either directly participate in the dimer interface (Figure 3E, teal) or are adjacent to the former, presumably reflecting allosteric effects (sand) (Figure S1C, III, top, e.g., stem, α13_{PBD}, and the IRA1 second helix). The kinked middle region of the scaffold showed suppressed dynamics (purple) (Figure S4D).

ADP rigidifies SecA₂ and mSecA local dynamics but not clamp motion

Cytoplasmic SecA₂ exists in a highly stable ADP state (Kerami-sanou et al., 2006; Sianidis et al., 2001). HDX-MS analysis demonstrated that ADP extensively stabilized multiple regions

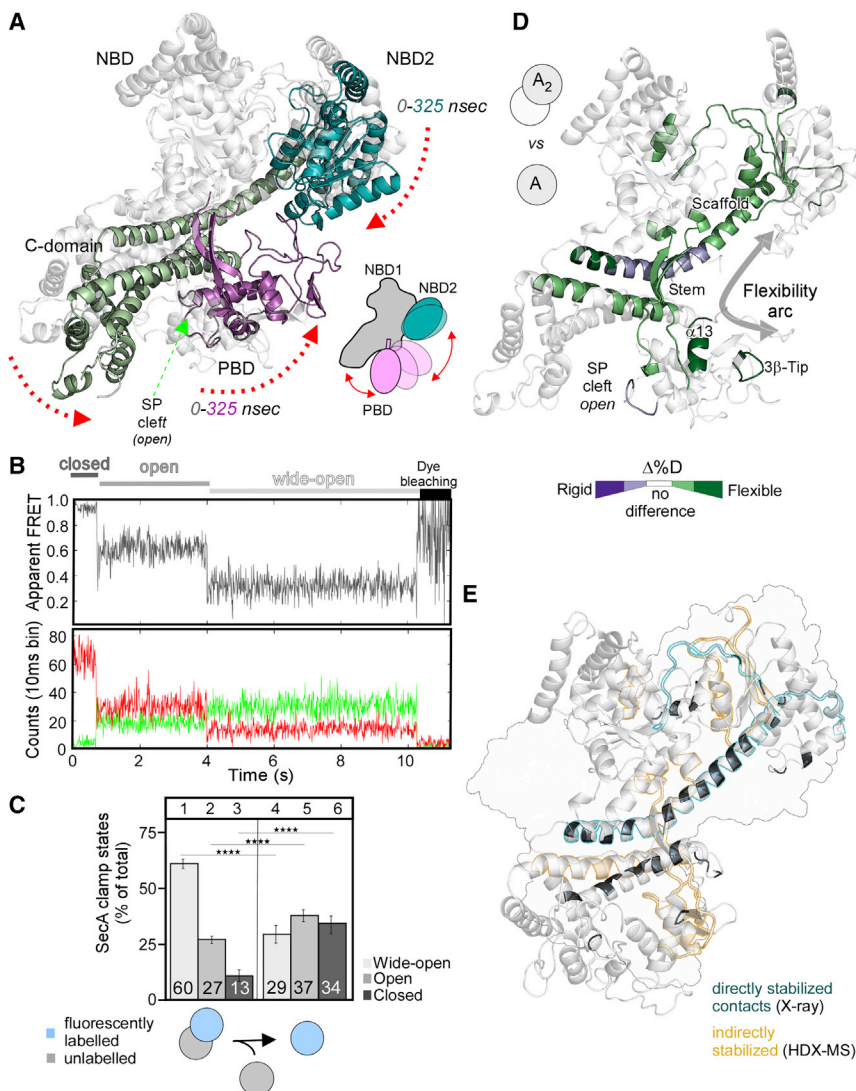


Figure 3. Effect of SecA monomerization on its domain and local dynamics

(A) Two coordinate snapshots from the start (0 ns; gray) and the end (325 ns) of the MD simulations of monomeric *ecSecA*_{2VDA} (PDB:2VDA) aligned based on their NBD1 (gray). Domains colored as in Figure 2A (see also Figures S2G and S2H).

(B) Top: representative FRET trace (1 of 84) of monomeric SecA. Bottom: photon counts collected during FRET trace recording.

(C) Clamp states quantified from solution smFRET of SecA₂ with a single fluorescently labeled protomer (lanes 1–3) or fluorescently labeled monomers (50–100 pM, lanes 4–6), as in Figure 2D; $n \geq 6$ biological repeats; mean \pm SEM (see also Figures S3A, S3B, and S6A). **** $p \leq 0.0001$.

(D) Effect of monomerization on local dynamics of SecA (see also Figure S5A). D-uptake differences (light and dark hues, $\Delta D = 10\%$ – 20% and $>20\%$, respectively) between the indicated dimer/monomer end states (control, dimer; test, monomer) are colored on the *ecSecA*_{2VDA} structure (top; decreased/increased dynamics, purple/green, respectively; no difference, white). Gray arrow, flexibility arc.

(E) Regions of a SecA protomer stabilized in SecA₂ either directly (involved in dimerization; *ecSecA*_{1M6N} (PDB:1M6N) X-ray structure, black/teal) or indirectly (from Figure 3D, sand), as indicated.

equilibrium toward stabilization and catalytic autoinhibition, while monomerization drives it toward a conformationally more dynamic and, presumably, functionally activated state.

Stem dynamics are expected to regulate PBD motions and thus clamp dynamics. Remarkably, while ADP binding marginally strengthened the preexisting contacts of the already predominant wide-open state of SecA₂ (Figure 4D,

compare lanes 4–6 with 1–3; Figures S3C, S3D, and S6B) it had no effect on monomeric SecA (compare lanes 10–12 with 7–9). In other words, the intrinsic PBD rotation occurs irrespective of the nucleotide state of the motor. This suggested that in monomeric SecA additional factors are required to couple the local dynamics of the nucleotide binding cleft to clamp motions.

ADP binds asymmetrically to the protomers of cytoplasmic SecA₂

In the two SecA₂ derivatives analyzed by MD simulations, the intradomain H-bonding networks within each of the four domains in each protomer are similar (Figures S2B–S2D). Nevertheless, they also revealed some detectable differences suggesting that, despite their similarities, the two protomers of the dimer retain some degree of structural asymmetry. To test if this reflects on the interaction of ADP with each protomer, we monitored the binding of ADP with the environmentally sensitive fluorescent probe MANT (2'-(or-3')-O-(*N*-methylanthraniloyl); Galletto et al., 2000; Karamanou et al., 2005).

in SecA₂ (Figures 4A and S5A, II). As most of these are also stabilized in mSecA (Figures 4B and S5A, III), the ADP effects are primarily intraprotomeric.

The nucleotide binding cleft was stabilized by multiple direct contacts that ADP makes with the helicase motifs inside the cleft and the allosteric stabilization of more peripheral ones (Figures 4A, right, and S1C, I), driving disorder-to-order transitions (Keramisanou et al., 2006). ADP binding also stabilized allosterically regions of the flexibility arc that lie several nanometers away from the nucleotide: the scaffold (attached to the ATPase motor *in trans*) and the stem (rooted in NBD1), which associate with each other, and the PBD, which is an extension of the stem (Figure S1C, II). These regions provide a physical pathway for the motor to communicate with the clamp (Bondar et al., 2020). Moreover, the stem, α 13, and the 3 β tip were overstabilized only in SecA₂ (Figures 4C and S5A, IV), due to preexisting, interprotomeric contacts in the wide-open state that explain its stability (Figure S1C, II–III). ADP binding stabilizes regions that were destabilized by monomerization, implying antagonism between these two processes. ADP binding drives the conformational

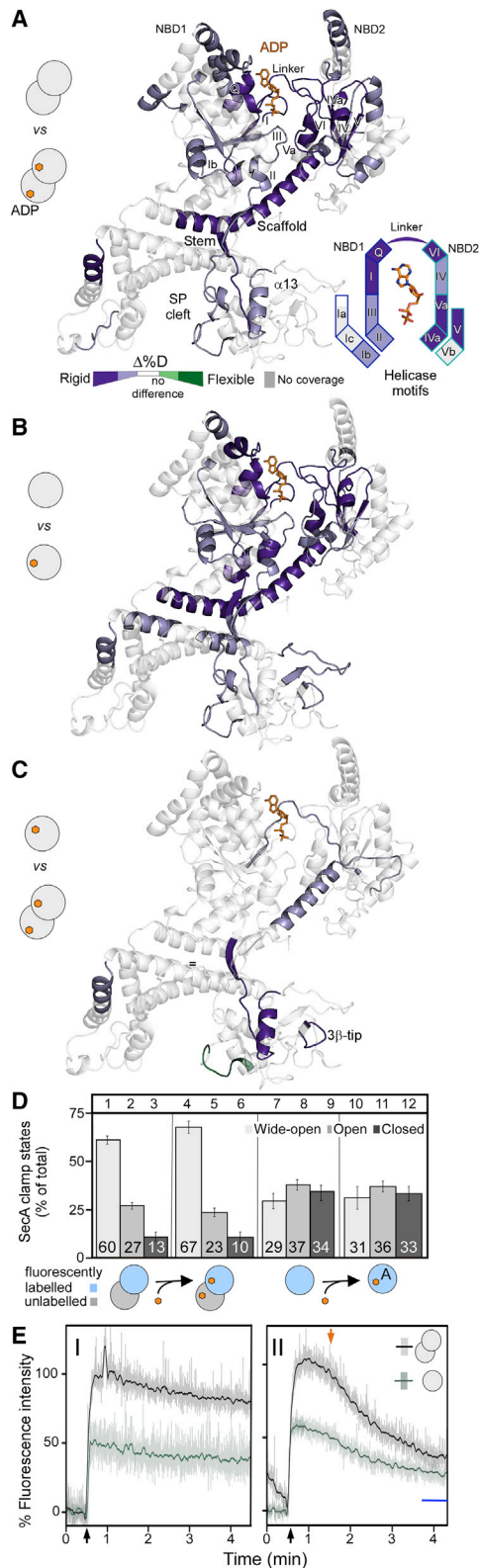


Figure 4. Effect of ADP on local and domain dynamics of SecA
(A and B) Pairwise comparisons of local dynamics determined by HDX-MS (as in Figure 3D) upon ADP (orange hexagon) binding on SecA₂ (A) or mSecA (B). To simplify comparison, data from both proteins have been mapped on

MANT-ADP rapidly binds to both SecA derivatives, reaching maximal intensities within 1 min and remaining very stably bound for several minutes. Given its provision of two binding sites, SecA₂ yields an ~2-fold higher intensity than does monomeric mSecA (Figure 4E, I). When chased with unlabeled ADP, the MANT-ADP bound to SecA₂ is approximately halved, while that of mSecA is significantly more stable and only partially exchanges (Figure 4E, II). These data suggested that after chase with excess unlabeled ADP, in SecA₂, one of the protomers retains a single MANT-ADP tightly bound, as does mSecA. In contrast, the other protomer readily exchanges ADP. These results together suggest that the two nucleotide binding clefts within SecA₂ display different functional properties and are therefore asymmetric. In contrast, SecA₂ mutants with constitutively elevated basal ATPase activity, and thus reduced ADP affinity, completely released the bound MANT-ADP (Figure 4E, II, blue line; Figure S7A).

We concluded that ADP binds to SecA₂ asymmetrically.

The stem is a central checkpoint of allosteric networks

The widespread responses to monomerization or ADP binding implied the existence of extensive allosteric networks across the protein. We probed them by graph analysis of the H-bonding networks derived from MD simulations. A large extended surface (Figure 5A) involving many SecA residues (~67%) that are interconnected via a dynamic water-mediated H-bond network was observed. The stem (Figure 5A, dashed lines) appears to be a critical linchpin, providing a narrow passage through which the ATPase motor communicates with the PBD. To better understand its role, we probed its structural contributions further.

The stem is an anti-parallel β sheet consisting of stem_{in} ($\beta 12$) and stem_{out} ($\beta 6$) of the PBD (Figure 5B), with which a third β strand ($\beta 24_{C-tail}$) associates (Hunt et al., 2002). All three β strands display enhanced dynamics but lean against the rigid $\alpha 8_{NBD1}$. While not essential for function or dimerization (Karamanou et al., 2005), $\beta 24$ occupies the binding site of client mature domains (Chatzi et al., 2017). Deleting the C tail of SecA₂ destabilized the wide-open state and led to clamp closing (Figures 5C, lanes 4–6, and Figure S6B, III–IV), along with increased local intrinsic dynamics in the flexibility arc (Figure S5B). Thus, $\beta 24_{C-tail}$ contributes to stem stabilization and restriction of clamp motions.

the ecSecA_{2VDA} open state (ribbon, left; PDB:2VDA) and a cartoon of the helicase motifs (right).

(C) Pairwise comparison of local dynamics of ADP-bound mSecA (control) and SecA₂ (test) to reveal the quantitative changes in dynamics that dimerization brings on top of those of ADP alone (see Figure S5A, IV).

(D) Quantification of clamp states from solution smFRET measurements comparing apo and ADP-bound SecA dimers (as in Figure 2D) or monomers (50–100 pM; as in Figure 2D). $n \geq 6$ biological repeats; mean \pm SEM. See also Figure S6A. Lanes 1–3, SecA₂; lanes 4–6, SecA₂:ADP; lanes 7–9, SecA; lanes 10–12, SecA:ADP.

(E) Fluorescence intensity of SecA₂ (0.5 μ M) or mSecA (1 μ M), added at 30 s (black arrow), binding to MANT-ADP (1 μ M) for 4.5 min. Raw fluorescence data (transparent lines) are superimposed on smoothed data (solid lines). The data were recorded for 4.5 min and normalized, taking the fluorescent signal of free MANT-ADP as 0% (I) and that of SecA₂-bound MANT-ADP as 100% (II; maximum fluorescence intensity). In II, MANT-ADP was chased with cold ADP (2 mM; added at 90 s; orange arrow). Blue line, percentage of fluorescence intensity level of elevated ATPase mutants after ADP chase (see Figure S7A for details).

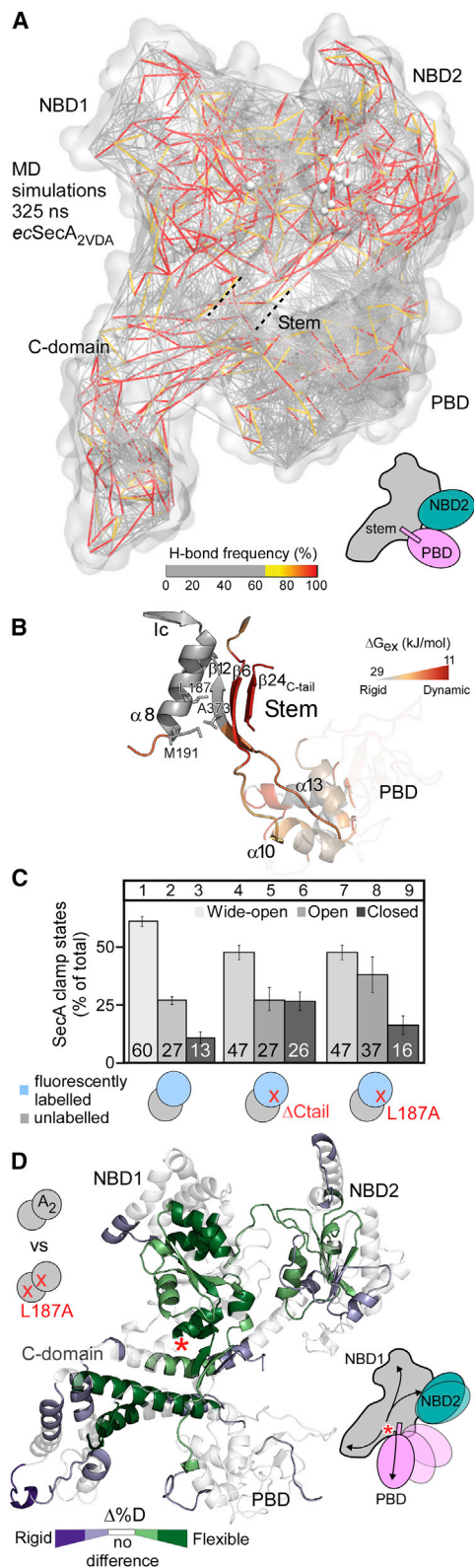


Figure 5. The stem regulates the intrinsic dynamics in SecA

(A) An H-bond protein-water network is shown for the loosely closed (325 ns) MD simulation of ecSecA₂VDA. Each line of the network represents one water-mediated H-bond bridge in the protein-water network

The stem and $\alpha 8_{\text{NBD1}}$ share a conserved hydrophobic interface, formed primarily by $\alpha 8_{\text{NBD1}}$ residues L187 and M191 and their juxtaposed A373 from stem_{in,PBD} (Figure 5B). While the stem as a whole is highly dynamic, the backbone of residues of $\beta 12$ of stem_{in}, which participate in the stem/ $\alpha 8$ interface, including that of A373, is rigid (Figure 5B). We hypothesized that this hydrophobic interface might be important for the stem to regulate local and clamp dynamics of SecA. To test this, we weakened the hydrophobic and bulk contribution of L187 by mutating it to alanine, so as to externally affect the stem without internally affecting the stem β strands. SecA₂(L187A) is functionally active and binds preproteins with an affinity similar to that of SecA₂ (Figures S7B and S7C). SecA₂(L187A) showed partial loss of the wide-open state and consequently clamp closing (Figures 5C, lanes 4–6, and S6B, V–VI).

Remarkably, the minor mutation in L187A (Figures 5D, red asterisk, and S5C) resulted in widespread allosteric responses, mostly increased local dynamics, radiating to almost all regions of SecA₂ (Figure 5D).

We concluded that the stem exploits the $\alpha 8$ /C-tail hydrophobic interactions to directly regulate both far-reaching intrinsic dynamics networks across SecA and clamp motions (Figure 5D, right).

Channel binding redistributes the clamp in active protomers of SecA₂

Having revealed the stem-controlled nexus of intrinsic dynamics that extends through most of the backbone of SecA, we set out to probe if it is influenced by channel binding to yield a translocase primed for preprotein secretion.

The channel carried in inverted inner membrane vesicles (IMVs) was added at stoichiometric excess over SecA, and its effect on clamp dynamics was probed. Channel binding shifts clamp equilibria from the wide-open to the open/closed states compared with freely diffusing SecA₂ (compare Figure 6A lanes 4–6 with 1–3; S6C, I–II), but not when it is influenced by channel binding to yield a translocase primed for preprotein secretion. Channel binding shifts clamp equilibria from the wide-open to the open/closed states compared with freely diffusing SecA₂ (compare Figure 6A lanes 4–6 with 1–3; S6C, I–II), but not when it is mutated for interaction with SecA₂ (SecY_{M15}; Figures 6A, lanes 7–9, and S6C, III) (Karamanou et al., 2008; Matsumoto et al., 2000). Therefore, the observed alteration of clamp equilibria caused by IMVs is specific to the channel. SecY_{M15} is a conditional mutant that carries a substitution in the carboxy-terminal C tail of SecY (Karamanou et al., 2008; Matsumoto et al., 2000). The SecY C tail has not been crystallographically resolved, but is apposed proximally to SecA, in the SecYEG:SecA complex (Figures S7D and S7E) (Zimmer et al., 2008) and binds SecA directly in a peptide array (Karamanou et al., 2008). These data suggested that a functional C tail is required for the channel to trigger clamp closing and signal peptide cleft exposure in SecA. It is important to note that this apparently occurs at a late stage

and is color coded based on frequency of appearance in the simulation.

(B) The stem- $\alpha 8$ interface structure and dynamics. The stem ($\beta 12$, $\beta 6$, and $\beta 24$) links to $\alpha 10$ and $\alpha 13$ of the PBD. $\alpha 8$ is an extension of helicase motif lc. ΔG_{ex} values of the stem region (from Figure 2E) are colored as indicated.

(C) Quantification of clamp states from solution smFRET comparing apoSecA₂ (lanes 1–3) with SecA(Δ Ctail)₂ (lanes 4–6) and SecA(L187A)₂ (lanes 7–9) (as in Figure 3C). $n \geq 6$ biological repeats; mean \pm SEM.

(D) Left: pairwise comparison of local dynamics of SecA₂ (control) against SecA(L187A)₂ (test) (as in Figure 3D; single protomer shown for simplicity). Right: cartoon of SecA(L187A)₂ (red asterisk) resulting in allosteric local effects that radiate to all SecA₂ domains (arrows) and affect clamp motions.

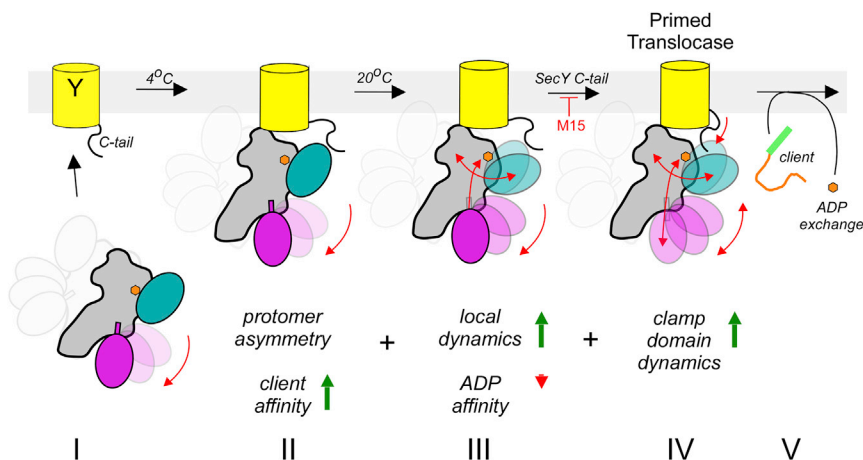


Figure 7. Model of translocase priming upon channel binding to SecA (see text for details)

Asymmetric binding of soluble SecA₂:ADP with a predominantly wide-open clamp to SecYEG is temperature independent and enhances local dynamics in SecA and loosening of the ADP cleft without ADP loss. At >20°C, via its C tail, SecY increases clamp dynamics to the bound SecA.

DISCUSSION

Translocase function is driven by multi-level intra- and intermolecular intrinsic dynamics. An excessively H-bonded framework of the SecA monomer comprising

the D-uptake values from the two asymmetric protomers of SecYEG:SecA₂:ADP.

Channel binding resulted in increased dynamics across multiple SecA₂:ADP regions (Figures 6D and S5D). The most characteristic effect was the partial reversal of the extensive ADP-driven stability that had been observed in soluble SecA₂:ADP (Figure 4B). This included enhanced dynamics in most helicase motifs of NBD2 and only in motifs I and Ib of NBD1 (Figures 6D and 6E). Despite the increased dynamics observed in many islands, the dynamics of the Q motif that anchors the adenine ring of ADP (Figure S1C, V) were unaltered, providing direct evidence that ADP remained bound. Corroborating this observation, no significant channel-driven release of MANT-ADP was detectable (Figures S7I and S7J). Increased dynamics predominantly in NBD2 and in the NBD1/NBD2 linker suggested that channel binding caused NBD2 to dissociate from NBD1 (Figure 6E). These dynamics are consistent with a helicase motor being primed by the channel for, but not yet performing, ATP catalysis (Keramisanou et al., 2006; Sianidis et al., 2001).

Elevated dynamics in the motor were directly transferred to the scaffold, stem, and most regions of the PBD (α 13, 3 β tip, and the signal peptide binding cleft). Stem and PBD elevated dynamics are coincident with the enhanced clamp mobility (Figure 6C, lanes 4–6).

To determine whether channel binding causes direct allosteric effects in addition to relieving those of ADP, we monitored the interactions of the SecA₂ apoprotein with the channel. Channel binding enhanced dynamics in two regions of SecA₂ (Figures 6F and S5D): NBD2 (motifs IV, V/Va, VI, and α 17 to which PBD binds in the closed state) and PBD (3 β tip, α 13_{PBD}, stem_{in}, and C tail). This further corroborated previous observations that channel binding results in NBD2 dynamics and liberates the clamp from the dimerization-imposed wide-open state (Figures 3C and S1C, III).

While the PBD distribution in the channel-bound active SecA protomer is reminiscent of that of monomeric SecA in solution, local dynamics of channel-bound SecA are nevertheless distinct from those of either free (Figure 6G) or channel-bound (Figure S5F) monomeric SecA, demonstrating that SecA remains dimeric upon binding the channel.

Channel-induced dynamics in SecA prime but do not activate the motor for subsequent nucleotide cycling, while the liberated clamp prepares the translocase for binding of preprotein clients.

flexible, distributed islands and domain motions yields a conformational repertoire of soft motion modes (Meireles et al., 2011; Zhang et al., 2020). These elements are controlled by external modulators that select preexisting attainable conformations and contribute their own dynamics: the second SecA protomer, nucleotides, the channel, and secretory clients. Such dynamics collectively support a conceptual departure from views of major ligand-biased enzyme motions between fixed start and end states to one of subtly balanced co-existing equilibria of dynamically interconverting states (Kumar et al., 2000; Ma et al., 1999). Such mechanisms are likely generic in multi-liganded protein machines.

We dissected this dynamic landscape in depth using a multi-pronged approach under similar conditions, on physiological membranes and under conditions in the absence of detergents. We linked specific intrinsic dynamics to translocase functional outcomes, i.e., the quiescent and the primed state. This pipeline sets the foundation for future studies of the translocase and other complex motors with dynamic clients, diffusing in solution or membrane-bound (Jang et al., 2019; Ramirez-Sarmiento and Komives, 2018).

Local and domain dynamics in SecA co-exist in multi-state equilibria facilitated by extensive H bonding (Figures 5A and S2; Table S2). Dynamics islands are sharply delimited (e.g., a few helical turns, half a β strand) and have escaped previous structural detection. They may act as either “on-off” switches (e.g., the ADP binding Walker A/motif I) or “rheostats” emanating gradients of dynamics to adjacent regions (e.g., the stem to the bulb). Different ligands target dynamics islands/domains differently and shift conformational equilibria; e.g., ADP affects dynamics islands in the helicase motor and scaffold but less so clamp motions.

All of the above establish an “intrinsic dynamics nexus” with distinct features at the heart of translocase catalysis. (1) As the nexus exploits the preexisting dynamics of monomeric SecA, minor free energy changes suffice for ligands to change enzyme states. We presume that this is also why ligand effects can be so easily recapitulated by point mutations that mimic signal peptide effects (Pri; Silhavy and Mitchell, 2019) or others that render the translocase temperature sensitive (Figure 6A) (Ito et al., 1983; Karamanou et al., 2008; Pogliano and Beckwith, 1993). (2) The multiplicity of dynamics nodes ensures that SecA responds to

multiple ligands, each incrementally changing its dynamics. Presumably, this also allows, in the next steps of the translocation reaction, the coupling of nucleotide cycling in the motor to client cycling on-off SecA and their threading through the channel. (3) Long-range effects are transmitted nanometers away from a ligand interaction site as seen prominently with ADP.

Dimerization prevents monomeric SecA from expressing its excessive dynamics prematurely. This created a stable, cytoplasmically diffusing quiescent cytoplasmic state with a mainly wide-open clamp and reduced client affinity (Figures 2C and 2D and 7, I). The two protomers of the same dimer display dynamics differences between them (Figure S2), and therefore protomer asymmetry may predispose them to stochastic SecY binding. Channel binding partially relieves these suppressed dynamics in the active protomer to which it binds and weakens the protomer-protomer interface while retaining dimerization (Figure 7, III). This allows a free tri-state clamp distribution in the active protomer (Figure 7, IV) and prepares the motor for ADP release (Figures 6A–6C and 7, V). The smFRET data revealed that the clamp in the monomeric SecA apoprotein occupies three near-isoenergetic troughs separated by activation energy barriers (Figure 3C). Dimerization elevates the wide-open/open energy barrier and traps the clamp in a stable wide-open state. In contrast, the simulated MD environment revealed a presumably energetically favored open to loosely closed equilibrium shift in monomeric SecA (Figure 3A; Video S1). Crossing this energetic barrier in smFRET experiments presumably requires the presence of both membranes and preproteins.

ADP is a top-level extrinsic regulator. It suppresses helicase motor and scaffold dynamics and hyperstabilizes the wide-open clamp, ensuring that SecA₂ remains quiescent in the cytoplasm (Figure 4A) and even on the channel, prior to client arrival. The main consequence of channel-induced priming is to reverse these effects to allow the free intrinsic motion of the clamp and loosen the ADP-induced restricted dynamics. In a demonstration of remarkable fine-tuning, and despite its acquisition of enhanced dynamics, the helicase motor retains ADP bound as evidenced by critical helicase motifs remaining stabilized (Figure 6D) and fluorescence assays (Figures S7I and S7J) and retains the ADP-bound asymmetry of SecA₂. This explains how the ATPase activity of SecA₂ is not significantly stimulated upon channel binding (Karamanou et al., 2007). Excessive stimulation will occur only once the preprotein clients bind, presumably by overcoming a significant energetic obstacle driving ADP release (Figure 7, V). In quiescent cytoplasmic SecA₂:ADP, a stable wide-open clamp with its associated C tail might impede mature domain access to the binding site (Chatzi et al., 2017), fending off unwanted cytoplasmic binders.

Protein structures are selected because their scaffolds successfully mediate specific surface chemistries. Intrinsic dynamics networks may drive their further evolution (Tiwari and Reuter, 2018; Zhang et al., 2020). Our data raise the possibility that a protein may be selected primarily because of its intrinsic dynamics propensities and then adapted to specific chemistries. The structurally conserved DEAD-box superfamily helicases, to which SecA belongs, share sequence conservation only in the helicase motifs (Jarmoskaite and Russell, 2014; Linder and Janowski, 2011; Papanikou et al., 2007). These motifs, many of them in weak internal parallel β sheets (Fairman-Williams et al.,

2010; Keramisanou et al., 2006; Sianidis et al., 2001), are all intrinsically dynamic (Figures 2E and 2F). Such dynamics are client chemistry agnostic. The ancestral helicase motor was presumably effective in reshaping the conformational states of dynamic clients, commonly nucleic acids, albeit promiscuously and inefficiently. SecA evolved to apply the ancestral helicase motor intrinsic dynamics to aminoacyl polymer chemistries. It did this by incorporating one specificity domain that reshapes dynamic non-folded polypeptides and binds signal peptides and another that brought this chemistry to the SecY channel by associating with it.

STAR★METHODS

Detailed methods are provided in the online version of this paper and include the following:

- KEY RESOURCES TABLE
- RESOURCE AVAILABILITY
 - Lead contact
 - Materials availability
 - Data and code availability
- EXPERIMENTAL MODEL AND SUBJECT DETAILS
- METHOD DETAILS
 - Molecular dynamics simulations
 - H-bond graphs and long-distance conformational coupling
 - Molecular cloning
 - Protein purification
 - Fluorescent labeling of SecA and sample preparation for smFRET and PIE
 - Single-molecule fluorescence microscopy and PIE
 - PIE data analysis
 - Confocal scanning microscopy and data analysis
 - Amide hydrogen/deuterium exchange mass spectrometry
 - Peptide identification and HDX data analysis
 - Binding of MANT-ADP to the SecA subunit of the translocase
 - Miscellaneous
- QUANTIFICATION AND STATISTICAL ANALYSIS
 - Quantification and statistical analysis for FRET data
 - HDX-MS data interpretation and visualization

SUPPLEMENTAL INFORMATION

Supplemental information can be found online at <https://doi.org/10.1016/j.str.2021.03.015>.

ACKNOWLEDGMENTS

This paper is dedicated to the memory of Yiannis Papanikolaou, who solved the first *E. coli* SecA structure. We are grateful to M. Papanastasiou for preliminary HDX-MS analysis of SecA; A. Tsirigotaki, M.B. Trelle, and J.T.D. Jorgensen for discussions and advice; T. Cordes for sharing software for smFRET data analysis; and V. Krasnikov for advice in setting up the smFRET microscope. Research in the Economou lab was funded by grants (to A.E.) RiMemBR (Vlaanderen Onderzoeksprojecten; G0C6814N; FWO); MeNaGe (RUN RUN/16/001; KU Leuven); ProFlow (FWO/F.R.S.-FNRS "Excellence of Science-EOS" program grant 30550343); DIP-BiD (AKUL/15/40-G0H2116N; Hercules/FWO); PROFOUND (Protein Folding/Un-folding and Dynamics;

W002421N; WoG/FWO) and (to A.E. and S.K.) FOscil (ZKD4582-C16/18/008; KU Leuven) and (to A.E. and G.G.): CARBS (G0C6814N; FWO). Funds for the smFRET microscope were from ZKD4582 and Economou lab resources. Research in the lab of A.-N.B. was supported in part by the Excellence Initiative of the German federal and state governments via the Freie Universität Berlin, and by allocations of computing time from the North-German Supercomputing Alliance, HLRN. G.G. was funded by the NWO (Veni grant 722.012.012), the Zernike Institute for Advanced Materials, and the Rega Foundation postdoctoral program; S.Kr. was an FWO [PEGASUS]² MSC fellow, J.H.S. is a PDM/KU Leuven fellow, and N.E. is an MSCA SoE FWO fellow. This project has received funding from the Research Foundation Flanders (FWO) and the European Union's Horizon 2020 Research and Innovation Programme under Marie Skłodowska-Curie grant agreements 665501 and 195872.

AUTHOR CONTRIBUTIONS

S.Kr. purified proteins and membranes, did biochemical assays, designed and performed HDX-MS work and data analysis, and performed ADP release assays and homology analysis. N.E. purified and labeled proteins and performed smFRET calibrations and experiments and data analysis, analyzed structures, and made movies. K.K. performed MD simulations and graph analysis of H-bond networks. J.H.S. developed the PyHDX software and adapted FRET burst analysis for Microtime200 output data. A.G.P. produced the HDX-MS and smFRET constructs by molecular cloning and mutagenesis. K.E.C. performed molecular biology and *in vivo* assays. S.K. designed and supervised molecular biology experiments and smFRET constructs, purified proteins for smFRET, and performed and supervised biochemical and biophysical assays and data analysis. A.N.B. set up and supervised the MD simulations and performed runs and data analysis. G.G. adapted the smFRET pipeline to Histagged SecA and designed the immobilized smFRET with major contributions from N.E.; technically supervised the smFRET work and the installation of the Microtime200 setup; performed molecular biology, biochemical, and biophysical assays; and analyzed data. A.E. designed experiments, did structure and data analysis, and performed biological/structural interpretation and integration of HDX-MS, smFRET, and MD data. A.E. and S.Kr. wrote the first draft with contributions from N.E., K.K., J.H.S., A.P., A.N.B., K.K., S.K., and G.G. All authors reviewed and approved the final manuscript. A.E. and S.K. conceived and managed the project.

DECLARATION OF INTERESTS

The authors declare they have no competing financial interests or other conflicts of interest.

Received: January 29, 2021

Revised: March 6, 2021

Accepted: March 25, 2021

Published: April 13, 2021

SUPPORTING CITATIONS

Amitai et al., 2004; Matsumoto et al., 1997; Roberts et al., 2006; Taura et al., 1997; Vrontou et al., 2004; Lazaratos et al., 2020; Mitchell and Oliver, 1993; Studier et al., 1990.

REFERENCES

Ahdash, Z., Pyle, E., Allen, W.J., Corey, R.A., Collinson, I., and Politis, A. (2019). HDX-MS reveals nucleotide-dependent, anti-correlated opening and closure of SecA and SecY channels of the bacterial translocon. *Elife* 8, e47402.

Allen, W.J., Corey, R.A., Oatley, P., Sessions, R.B., Baldwin, S.A., Radford, S.E., Tuma, R., and Collinson, I. (2016). Two-way communication between SecY and SecA suggests a Brownian ratchet mechanism for protein translocation. *Elife* 5, e15598.

Amitai, G., Shemesh, A., Sitbon, E., Shklar, M., Netanel, D., Venger, I., and Pietrokovski, S. (2004). Network analysis of protein structures identifies functional residues. *J. Mol. Biol.* 344, 1135–1146.

Avellaneda, M.J., Koers, E.J., Naqvi, M.M., and Tans, S.J. (2017). The chaparrone toolbox at the single-molecule level: from clamping to confining. *Protein Sci.* 26, 1291–1302.

Bauer, B.W., and Rapoport, T.A. (2009). Mapping polypeptide interactions of the SecA ATPase during translocation. *Proc. Natl. Acad. Sci. U S A* 106, 20800–20805.

Ben Chorin, A., Masrati, G., Kessel, A., Narunsky, A., Sprinzak, J., Lahav, S., Ashkenazy, H., and Ben-Tal, N. (2020). ConSurf-DB: an accessible repository for the evolutionary conservation patterns of the majority of PDB proteins. *Protein Sci.* 29, 258–267.

Bhabha, G., Biel, J.T., and Fraser, J.S. (2015). Keep on moving: discovering and perturbing the conformational dynamics of enzymes. *Acc. Chem. Res.* 48, 423–430.

de Boer, M., Gouridis, G., Vietrov, R., Begg, S.L., Schuurman-Wolters, G.K., Husada, F., Eleftheriadis, N., Poolman, B., McDevitt, C.A., and Cordes, T. (2019). Conformational and dynamic plasticity in substrate-binding proteins underlies selective transport in ABC importers. *Elife* 8, e44652.

Bondar, A.N., Mishima, H., and Okamoto, Y. (2020). Molecular movie of nucleotide binding to a motor protein. *Biochim. Biophys. Acta Gen. Subj.* 1864, 129654.

Brooks, B.R., Brucoleri, R.E., Olafson, B.D., States, D.J., Swaminathan, S., and Karplus, M. (1983). CHARMM: a program for macromolecular energy, minimization, and dynamics calculations. *J. Comput. Chem.* 4, 187–217.

Brown, K.A., and Wilson, D.J. (2017). Bottom-up hydrogen deuterium exchange mass spectrometry: data analysis and interpretation. *Analyst* 142, 2874–2886.

Catipovic, M.A., Bauer, B.W., Loparo, J.J., and Rapoport, T.A. (2019). Protein translocation by the SecA ATPase occurs by a power-stroke mechanism. *EMBO J.* 38, e101140.

Chatzi, K.I., Gouridis, G., Orfanoudaki, G., Koukaki, M., Tsamardinos, I., Karamanou, S., and Economou, A. (2011). The signal peptides and the early mature domain cooperate for efficient secretion. *FEBS J.* 278, 14.

Chatzi, K.E., Sardis, M.F., Tsigiotaki, A., Koukaki, M., Sostaric, N., Konijnenberg, A., Sobott, F., Kalodimos, C.G., Karamanou, S., and Economou, A. (2017). Preprotein mature domains contain translocase targeting signals that are essential for secretion. *J. Cell Biol.* 216, 1357–1369.

Corey, R.A., Ahdash, Z., Shah, A., Pyle, E., Allen, W.J., Fessl, T., Lovett, J.E., Politis, A., and Collinson, I. (2019). ATP-induced asymmetric pre-protein folding as a driver of protein translocation through the Sec machinery. *Elife* 8, e41803.

Cormen, T.H., Leiserson, C.E., Rivest, R.L., and Sten, C. (2009). Introduction to Algorithms, third edition (Massachusetts Institute of Technology).

Economou, A., and Wickner, W. (1994). SecA promotes preprotein translocation by undergoing ATP-driven cycles of membrane insertion and deinsertion. *Cell* 78, 835–843.

Eggeling, C., Berger, S., Brand, L., Fries, J.R., Schaffer, J., Volkmer, A., and Seidel, C.A. (2001). Data registration and selective single-molecule analysis using multi-parameter fluorescence detection. *J. Biotechnol.* 86, 163–180.

Ernst, I., Haase, M., Ernst, S., Yuan, S., Kuhn, A., and Leptihn, S. (2018). Large conformational changes of a highly dynamic pre-protein binding domain in SecA. *Commun. Biol.* 1, 130.

Fairman-Williams, M.E., Guenther, U.P., and Jankowsky, E. (2010). SF1 and SF2 helicases: family matters. *Curr. Opin. Struct. Biol.* 20, 313–324.

Fak, J.J., Itkin, A., Ciobanu, D.D., Lin, E.C., Song, X.J., Chou, Y.T., Gierasch, L.M., and Hunt, J.F. (2004). Nucleotide exchange from the high-affinity ATP-binding site in SecA is the rate-limiting step in the ATPase cycle of the soluble enzyme and occurs through a specialized conformational state. *Biochemistry* 43, 7307–7327.

Feller, S.E., Zhang, Y., Pastor, R.W., and Brooks, B. (1995). Constant pressure molecular dynamics simulation: the Langevin piston method. *J. Chem. Phys.* 103, 4613–4621.

Flechsigs, H., and Mikhailov, A.S. (2019). Simple mechanics of protein machines. *J. R. Soc. Interf.* 16, 20190244.

- Freeman, L.C. (1977). A set of measures of centrality based on betweenness. *Sociometry* **40**, 35–41.
- Freeman, L.C. (1979). Centrality in social networks. Conceptual clarification. *Soc. Netw.* **1**, 215–239.
- Galletto, R., Rajendran, S., and Bujalowski, W. (2000). Interactions of nucleotide cofactors with the *Escherichia coli* replication factor DnaC protein. *Biochemistry* **39**, 12959–12969.
- Gelis, I., Bonvin, A.M., Keramisanou, D., Koukaki, M., Gouridis, G., Karamanou, S., Economou, A., and Kalodimos, C.G. (2007). Structural basis for signal-sequence recognition by the translocase motor SecA as determined by NMR. *Cell* **131**, 756–769.
- De Geyter, J., Portaliou, A.G., Srinivasu, B., Krishnamurthy, S., Economou, A., and Karamanou, S. (2020). Trigger factor is a bona fide secretory pathway chaperone that interacts with SecB and the translocase. *EMBO Rep.* **21**, e49054.
- Gouridis, G., Karamanou, S., Gelis, I., Kalodimos, C.G., and Economou, A. (2009). Signal peptides are allosteric activators of the protein translocase. *Nature* **462**, 363–367.
- Gouridis, G., Karamanou, S., Koukaki, M., and Economou, A. (2010). In vitro assays to analyze translocation of the model secretory preprotein alkaline phosphatase. *Methods Mol. Biol.* **619**, 157–172.
- Gouridis, G., Karamanou, S., Sardis, M.F., Schärer, M.A., Capitani, G., and Economou, A. (2013). Quaternary dynamics of the SecA motor drive translocase catalysis. *Mol. Cell* **52**, 655–666.
- Gouridis, G., Schuurman-Wolters, G.K., Ploetz, E., Husada, F., Vietrov, R., de Boer, M., Cordes, T., and Poolman, B. (2015). Conformational dynamics in substrate-binding domains influences transport in the ABC importer GlnPQ. *Nat. Struct. Mol. Biol.* **22**, 57–64.
- Gouridis, G., Hetzert, B., Kiosze-Becker, K., de Boer, M., Heinemann, H., Nurenberg-Goloub, E., Cordes, T., and Tampe, R. (2019). ABCE1 controls ribosome recycling by an asymmetric dynamic conformational equilibrium. *Cell Rep.* **28**, 723–734.e6.
- Hellenkamp, B., Schmid, S., Doroshenko, O., Opanasyuk, O., Kuhnemuth, R., Rezaei Adariani, S., Ambrose, B., Aznauryan, M., Barth, A., Birkedal, V., et al. (2018). Precision and accuracy of single-molecule FRET measurements—a multi-laboratory benchmark study. *Nat. Methods* **15**, 669–676.
- Henzler-Wildman, K., and Kern, D. (2007). Dynamic personalities of proteins. *Nature* **450**, 964–972.
- Henzler-Wildman, K.A., Lei, M., Thai, V., Kerns, S.J., Karplus, M., and Kern, D. (2007). A hierarchy of timescales in protein dynamics is linked to enzyme catalysis. *Nature* **450**, 913–916.
- Houde, D., Berkowitz, S.A., and Engen, J.R. (2011). The utility of hydrogen/deuterium exchange mass spectrometry in biopharmaceutical comparability studies. *J. Pharm. Sci.* **100**, 2071–2086.
- Hu, W., Walters, B.T., Kan, Z.Y., Mayne, L., Rosen, L.E., Marqusee, S., and Englander, S.W. (2013). Stepwise protein folding at near amino acid resolution by hydrogen exchange and mass spectrometry. *Proc. Natl. Acad. Sci. U S A* **110**, 7684–7689.
- Humphrey, W., Dalke, A., and Schulten, K. (1996). VMD: visual molecular dynamics. *J. Mol. Graph.* **14**, 33–38, 27–38.
- Hunt, J.F., Weinkauff, S., Henry, L., Fak, J.J., McNicholas, P., Oliver, D.B., and Deisenhofer, J. (2002). Nucleotide control of interdomain interactions in the conformational reaction cycle of SecA. *Science* **297**, 2018–2026.
- Ito, K., Wittekind, M., Nomura, M., Shiba, K., Yura, T., Miura, A., and Nashimoto, H. (1983). A temperature-sensitive mutant of *E. coli* exhibiting slow processing of exported proteins. *Cell* **32**, 789–797.
- Jang, S., Kang, C., Yang, H.S., Jung, T., Hebert, H., Chung, K.Y., Kim, S.J., Hohng, S., and Song, J.J. (2019). Structural basis of recognition and destabilization of the histone H2B ubiquitinated nucleosome by the DOT1L histone H3 Lys79 methyltransferase. *Genes Dev.* **33**, 620–625.
- Jarmoskaite, I., and Russell, R. (2014). RNA helicase proteins as chaperones and remodelers. *Annu. Rev. Biochem.* **83**, 697–725.
- Jo, S., and Kim, T. (2008). CHARMM-GUI Solvator. <https://charmm-gui.org/>.
- Jo, S., Kim, T., Iyer, V.G., and Im, W. (2008). CHARMM-GUI: a web-based graphical user interface for CHARMM. *J. Comput. Chem.* **29**, 1859–1865.
- Jorgensen, W.L., Chandrasekhar, J., Madura, J.D., Impey, R.W., and Klein, M.L. (1983). Comparison of simple potential functions for simulating liquid water. *J. Chem. Phys.* **79**, 926–935.
- Kalé, L., Skeel, R., Bhandarkar, M., Brunner, R., Gursoy, A., Krawetz, N., Phillips, J., Shinozaki, A., Varadarajan, K., and Schulten, K. (1999). NAMD2: greater scalability for parallel molecular dynamics. *J. Comput. Phys.* **151**, 283–312.
- Kapanidis, A.N., Lee, N.K., Laurence, T.A., Doose, S., Margeat, E., and Weiss, S. (2004). Fluorescence-aided molecule sorting: analysis of structure and interactions by alternating-laser excitation of single molecules. *Proc. Natl. Acad. Sci. U S A* **101**, 8936–8941.
- Karamanou, S., Sianidis, G., Gouridis, G., Pozidis, C., Papanikolaou, Y., Papanikou, E., and Economou, A. (2005). *Escherichia coli* SecA truncated at its termini is functional and dimeric. *FEBS Lett.* **579**, 1267–1271.
- Karamanou, S., Gouridis, G., Papanikou, E., Sianidis, G., Gelis, I., Keramisanou, D., Vrontou, E., Kalodimos, C.G., and Economou, A. (2007). Preprotein-controlled catalysis in the helicase motor of SecA. *EMBO J.* **26**, 2904–2914.
- Karamanou, S., Bariami, V., Papanikou, E., Kalodimos, C.G., and Economou, A. (2008). Assembly of the translocase motor onto the preprotein-conducting channel. *Mol. Microbiol.* **70**, 311–322.
- Karathanou, Konstantina (2020). Centrality measures and H-bond clustering in proteins. *Mendeley Data*, V1, <https://doi.org/10.17632/wbprcvz6h2.1>.
- Karathanou, K., and Bondar, A.N. (2018). Dynamic water hydrogen-bond networks at the interface of a lipid membrane containing palmitoyl-oleoyl phosphatidylglycerol. *J. Membr. Biol.* **251**, 461–473.
- Karathanou, K., and Bondar, A.N. (2019). Using graphs of dynamic hydrogen-bond networks to dissect conformational coupling in a protein motor. *J. Chem. Inf. Model.* **59**, 1882–1896.
- Keramisanou, D., Biris, N., Gelis, I., Sianidis, G., Karamanou, S., Economou, A., and Kalodimos, C.G. (2006). Disorder-order folding transitions underlie catalysis in the helicase motor of SecA. *Nat. Struct. Mol. Biol.* **13**, 594–602.
- Kumar, S., Ma, B., Tsai, C.J., Sinha, N., and Nussinov, R. (2000). Folding and binding cascades: dynamic landscapes and population shifts. *Protein Sci.* **9**, 10–19.
- Kurakin, A. (2006). Self-organization versus watchmaker: molecular motors and protein translocation. *Biosystems* **84**, 15–23.
- Lazaratos, M., Karathanou, K., and Bondar, A.N. (2020). Graphs of dynamic H-bond networks: from model proteins to protein complexes in cell signaling. *Curr. Opin. Struct. Biol.* **64**, 79–87.
- Lill, R., Cunningham, K., Brundage, L.A., Ito, K., Oliver, D., and Wickner, W. (1989). SecA protein hydrolyzes ATP and is an essential component of the protein translocation ATPase of *Escherichia coli*. *EMBO J.* **8**, 961–966.
- Lill, R., Dowhan, W., and Wickner, W. (1990). The ATPase activity of SecA is regulated by acidic phospholipids, SecY, and the leader and mature domains of precursor proteins. *Cell* **60**, 271–280.
- Linder, P., and Jankowsky, E. (2011). From unwinding to clamping - the DEAD box RNA helicase family. *Nat. Rev. Mol. Cell Biol.* **12**, 505–516.
- Loutchko, D., and Flechsig, H. (2020). Allosteric communication in molecular machines via information exchange: what can be learned from dynamical modeling. *Biophys. Rev.* **12**, 443–452.
- Ma, B., Kumar, S., Tsai, C.J., and Nussinov, R. (1999). Folding funnels and binding mechanisms. *Protein Eng.* **12**, 713–720.
- Ma, C., Wu, X., Sun, D., Park, E., Catipovic, M.A., Rapoport, T.A., Gao, N., and Li, L. (2019). Structure of the substrate-engaged SecA-SecY protein translocation machine. *Nat. Commun.* **10**, 2872.
- MacKerell, A.D., Jr., Bashford, D., Bellot, M., Dunbrack, R.L., Evanseck, J.D., Field, M.J., Fischer, S., Gao, J., Guo, H., Ha, S., et al. (1998). All-atom empirical potential for molecular modeling and dynamics studies of proteins. *J. Phys. Chem. B* **102**, 3586–3616.

- MacKerell, A.D., Jr., Feig, M., and Brooks, C.L.I. (2004). Extending the treatment of backbone energetics in protein force fields: limitations of gas-phase quantum mechanics in reproducing protein conformational distributions in molecular dynamics simulations. *J. Comput. Chem.* **25**, 1400–1415.
- Martyna, G.J., Tobias, D.J., and Klein, M.L. (1994). Constant-pressure molecular-dynamics algorithms. *J. Chem. Phys.* **101**, 4177–4189.
- Masson, G.R., Burke, J.E., Ahn, N.G., Anand, G.S., Borchers, C., Brier, S., Bou-Assaf, G.M., Engen, J.R., Englander, S.W., Faber, J., et al. (2019). Recommendations for performing, interpreting and reporting hydrogen deuterium exchange mass spectrometry (HDX-MS) experiments. *Nat. Methods* **16**, 595–602.
- Matsumoto, G., Yoshihisa, T., and Ito, K. (1997). SecY and SecA interact to allow SecA insertion and protein translocation across the Escherichia coli plasma membrane. *EMBO J.* **16**, 6384–6393.
- Matsumoto, G., Nakatogawa, H., Mori, H., and Ito, K. (2000). Genetic dissection of SecA: suppressor mutations against the secY205 translocase defect. *Genes Cells* **5**, 991–999.
- Meireles, L., Gur, M., Bakan, A., and Bahar, I. (2011). Pre-existing soft modes of motion uniquely defined by native contact topology facilitate ligand binding to proteins. *Protein Sci.* **20**, 1645–1658.
- Mitchell, C., and Oliver, D. (1993). Two distinct ATP-binding domains are needed to promote protein export by Escherichia coli SecA ATPase. *Mol. Microbiol.* **10**, 483–497.
- Muller, B.K., Zaychikov, E., Brauchle, C., and Lamb, D.C. (2005). Pulsed interleaved excitation. *Biophys. J.* **89**, 3508–3522.
- Nir, E., Michalet, X., Hamadani, K.M., Laurence, T.A., Neuhauser, D., Kovchegov, Y., and Weiss, S. (2006). Shot-noise limited single-molecule FRET histograms: comparison between theory and experiments. *J. Phys. Chem. B* **110**, 22103–22124.
- Papanikolaou, Y., Papadovasilaki, M., Ravelli, R.B., McCarthy, A.A., Cusack, S., Economou, A., and Petratos, K. (2007). Structure of dimeric SecA, the Escherichia coli preprotein translocase motor. *J. Mol. Biol.* **366**, 1545–1557.
- Papanikou, E., Karamanou, S., and Economou, A. (2007). Bacterial protein secretion through the translocase nanomachine. *Nat. Rev. Microbiol.* **5**, 839–851.
- Phillips, J.C., Braun, B., Wang, W., Gumbart, J., Tajkhorshid, E., Villa, E., Chipot, C., Skeel, R.D., Kale, L., and Schulten, K. (2005). Scalable molecular dynamics with NAMD. *J. Comput. Chem.* **26**, 1781–1802.
- Ploetz, E., Lerner, E., Husada, F., Roelfs, M., Chung, S., Hohlbein, J., Weiss, S., and Cordes, T. (2016). Forster resonance energy transfer and protein-induced fluorescence enhancement as synergetic multi-scale molecular rulers. *Sci. Rep.* **6**, 33257.
- Pogliano, K.J., and Beckwith, J. (1993). The Cs sec mutants of Escherichia coli reflect the cold sensitivity of protein export itself. *Genetics* **133**, 763–773.
- Ramirez-Sarmiento, C.A., and Komives, E.A. (2018). Hydrogen-deuterium exchange mass spectrometry reveals folding and allostery in protein-protein interactions. *Methods* **144**, 43–52.
- Rapoport, T.A., Li, L., and Park, E. (2017). Structural and mechanistic insights into protein translocation. *Annu. Rev. Cell Dev Biol* **33**, 369–390.
- Roberts, E., Eargle, J., Wright, D., and Luthey-Schulten, Z. (2006). MultiSeq: unifying sequence and structure data for evolutionary analysis. *BMC Bioinformatics* **7**, 382.
- Sardis, M.F., and Economou, A. (2010). SecA: a tale of two protomers. *Mol. Microbiol.* **76**, 1070–1081.
- Sharma, V., Arockiasamy, A., Ronning, D.R., Savva, C.G., Holzenburg, A., Braunstein, M., Jacobs, W.R., Jr., and Sacchettini, J.C. (2003). Crystal structure of Mycobacterium tuberculosis SecA, a preprotein translocating ATPase. *Proc. Natl. Acad. Sci. U S A* **100**, 2243–2248.
- Sianidis, G., Karamanou, S., Vrontou, E., Boulias, K., Repanas, K., Kyrpides, N., Politou, A.S., and Economou, A. (2001). Cross-talk between catalytic and regulatory elements in a DEAD motor domain is essential for SecA function. *EMBO J.* **20**, 961–970.
- Silhavy, T.J., and Mitchell, A.M. (2019). Genetic analysis of protein translocation. *Protein J.* **38**, 217–228.
- Skinner, J.J., Lim, W.K., Bedard, S., Black, B.E., and Englander, S.W. (2012). Protein hydrogen exchange: testing current models. *Protein Sci.* **21**, 987–995.
- Smit, J.H., Krishnamurthy, S., Srinivasu, B.Y., Karamanou, S., and Economou, A. (2020). PyHDX: derivation and visualization of protection factors from Hydrogen-Deuterium Exchange Mass Spectrometry at near residue resolution. *bioRxiv*. <https://doi.org/10.1101/2020.09.30.320887>.
- Studier, F.W., Rosenberg, A.H., Dunn, J.J., and Dubendorff, J.W. (1990). Use of T7 RNA polymerase to direct expression of cloned genes. *Methods Enzymol.* **185**, 60–89.
- Taura, T., Yoshihisa, T., and Ito, K. (1997). Protein translocation functions of Escherichia coli SecY: in vitro characterization of cold-sensitive secY mutants. *Biochimie* **79**, 517–521.
- Tiwari, S.P., and Reuter, N. (2018). Conservation of intrinsic dynamics in proteins—what have computational models taught us? *Curr. Opin. Struct. Biol.* **50**, 75–81.
- Tsirigotaki, A., De Geyter, J., Sostaric, N., Economou, A., and Karamanou, S. (2017a). Protein export through the bacterial Sec pathway. *Nat. Rev. Microbiol.* **15**, 21–36.
- Tsirigotaki, A., Papanastasiou, M., Trelle, M.B., Jorgensen, T.J., and Economou, A. (2017b). Analysis of translocation-competent secretory proteins by HDX-MS. *Methods Enzymol.* **586**, 57–83.
- Vadas, O., and Burke, J.E. (2015). Probing the dynamic regulation of peripheral membrane proteins using hydrogen deuterium exchange-MS (HDX-MS). *Biochem. Soc. Trans.* **43**, 773–786.
- Vandenberk, N., Karamanou, S., Portaliou, A.G., Zorzini, V., Hofkens, J., Hendrix, J., and Economou, A. (2019). The preprotein binding domain of SecA displays intrinsic rotational dynamics. *Structure* **27**, 90–101.e6.
- Vrontou, E., Karamanou, S., Baud, C., Sianidis, G., and Economou, A. (2004). Global co-ordination of protein translocation by the SecA IRA1 switch. *J. Biol. Chem.* **279**, 22490–22497.
- Wales, T.E., Eggertson, M.J., and Engen, J.R. (2013). Considerations in the analysis of hydrogen exchange mass spectrometry data. *Methods Mol. Biol.* **1007**, 263–288.
- Walters, B.T., Ricciuti, A., Mayne, L., and Englander, S.W. (2012). Minimizing back exchange in the hydrogen exchange-mass spectrometry experiment. *J. Am. Soc. Mass Spectrom.* **23**, 2132–2139.
- Wowor, A.J., Yu, D., Kendall, D.A., and Cole, J.L. (2011). Energetics of SecA dimerization. *J. Mol. Biol.* **408**, 87–98.
- Wowor, A.J., Yan, Y., Auclair, S.M., Yu, D., Zhang, J., May, E.R., Gross, M.L., Kendall, D.A., and Cole, J.L. (2014). Analysis of SecA dimerization in solution. *Biochemistry* **53**, 3248–3260.
- Yang, L.Q., Sang, P., Tao, Y., Fu, Y.X., Zhang, K.Q., Xie, Y.H., and Liu, S.Q. (2014). Protein dynamics and motions in relation to their functions: several case studies and the underlying mechanisms. *J. Biomol. Struct. Dyn.* **32**, 372–393.
- Zhang, Y., Doruker, P., Kaynak, B., Zhang, S., Krieger, J., Li, H., and Bahar, I. (2020). Intrinsic dynamics is evolutionarily optimized to enable allosteric behavior. *Curr. Opin. Struct. Biol.* **62**, 14–21.
- Zimmer, J., Nam, Y., and Rapoport, T.A. (2008). Structure of a complex of the ATPase SecA and the protein-translocation channel. *Nature* **455**, 936–943.

STAR★METHODS

KEY RESOURCES TABLE

REAGENT or RESOURCE	SOURCE	IDENTIFIER
Bacterial and virus strains		
DH5 α : <i>F- endA1 glnV44 thi-1 recA1 relA1 gyrA96 deoR nupG purB20 ϕ80dlacZΔM15 Δ(lacZYA-argF)U169, hsdR17(rK-mK+), λ-</i>	Invitrogen	Cat# 18258012
BL21 (DE3): T7 RNA polymerase gene under the control of the <i>lac</i> UV5 promoter	(Studier et al., 1990)	N/A
BL21.19 (DE3): <i>secA13(Am) clpA::kan, ts</i> at 42°C;	(Mitchell and Oliver, 1993)	N/A
BL31 (DE3): Non <i>ts</i> ; spontaneous revertant of BL21.19 (DE3)	(Chatzi et al., 2017)	N/A
Chemicals, peptides, and recombinant proteins		
Tris base	Sigma-Aldrich	Cat# T1378
NaCl	Sigma-Aldrich	Cat# 7647-14-5
Magnesium Chloride (MgCl ₂)	Roth	Cat# 2189
Zinc Sulphate heptahydrate (ZnSO ₄)	Roth	Cat# 7316.1
Ethylenediaminetetraaceticacid, diNa salt, 2aq (EDTA)	ChemLab	Cat# CL00.0503
Phenylmethylsulfonylfluoride (PMSF)	Roth	Cat# 6367
Dithiothreitol (DTT)	ApplichemPanreac	Cat# A1101
Trolox	Sigma-Aldrich	Cat# 53188-07-1
Alexa Fluor 555 C ₂ Maleimide	Thermo Fisher Scientific	Cat# A20346
Alexa Fluor 647 C ₂ Maleimide	Thermo Fisher Scientific	Cat# A20347
ADP (Adenosine 5'-Diphosphate)	Sigma-Aldrich	Cat# A2754
MANT-ADP (2'- (or-3') - O - (N -Methylantraniloyl) Adenosine 5'-Diphosphate, Disodium Salt)	Invitrogen/ Thermo Fisher Scientific	Cat# M12416
TCEP ([Tris(2-carboxyethyl)phosphine])	Sigma-Aldrich	Cat# 51805-45-9
Bio-Rad Protein assay dye reagent	Bio-Rad	Cat# 5000006
Urea-d4 (98% D)	Sigma	Cat# 176087
Formic Acid (Ultra-pure)	Sigma-Aldrich	Cat# 330020050
PFU Ultra Polymerase	Promega	Cat# M7741
Dpn1	Promega	Cat# R6231
NdeI	Promega	Cat# R6801
BamHI	Promega	Cat# R6021
Acetonitrile	Merck Millipore	Cat#1000291000
Fungal protease type XIII	Sigma-Aldrich	Cat# P2143
Immobilized pepsin resin	Thermo Fisher Scientific	Cat# 20343
Deuterium Oxide (99.9%)	Euroisotop	Cat# D216
Critical commercial assays		
QuickChange Site-directed mutagenesis protocol	Stratagene-Agilent	N/A
Plasmid purification (NucleoSpin® Plasmid EasyPure)	Macherey- Nagel	Cat# 740727
Deposited data		
Crystal structure of ADP-bound dimeric SecA from <i>Escherichia coli</i>	(Papanikolaou et al., 2007)	PDB: 2FSI
Crystal structure of dimeric SecA from <i>Bacillus subtilis</i>	(Hunt et al., 2002)	PDB: 1M6N

(Continued on next page)

Continued

REAGENT or RESOURCE	SOURCE	IDENTIFIER
Crystal structure of dimeric SecA from <i>Mycobacterium tuberculosis</i>	(Sharma et al., 2003)	PDB: 1NL3
Crystal structure of SecA:SecYEG complex	(Zimmer et al., 2008)	PDB: 3DIN
Crystal structure of SecA-signal peptide complex	(Gelis et al., 2007)	PDB: 2VDA

Oligonucleotides

For primers used in this study see [Table S6](#)

Recombinant DNA

For vectors used in this study see [Table S5](#)

For genetic constructs used in this study see [Table S5](#)

Software and algorithms

Masslynx V4.1	Waters	www.waters.com; RRID: SCR_014271
DynamX 3.0	Waters	www.waters.com
PyHDX 0.3.0	(Smit et al., 2020)	https://github.com/Jhsmit/PyHDX
ConSurf Database	(Ben Chorin et al., 2020)	https://consurfdb.tau.ac.il; RRID: SCR_002320
Origin	OriginLab	https://www.originlab.com/index.aspx?go=Products/Origin
Matlab (R2014b/R2017b)	MathWorks	www.mathworks.com/products/matlab; RRID: SCR_001622
Pymol	Schrödinger	https://pymol.org/2/; RRID: SCR_000305
CHARMM-GUI	(Jo et al., 2008)	http://www.charmm-gui.org/
NAMD	(Phillips et al., 2005)	http://www.ks.uiuc.edu/Research/namd/; RRID: SCR_014894
Centrality measures and H-Bond clustering	Mendeley data-Karathanou, K. (2020)	https://data.mendeley.com/datasets/wbprcvz6h2/1
SymPhoTime 64	PicoQuant	www.picoquant.com
Alex suite	(Ploetz et al., 2016)	N/A
VMD 1.9.3	(Humphrey et al., 1996)	http://www.ks.uiuc.edu/Research/vmd/; RRID: SCR_001820
Clustal omega	EMBL-EBI	https://www.ebi.ac.uk/Tools/msa/clustalo/; RRID: SCR_001591
Prism 5.0	Graphpad	www.graphpad.com/scientific-software/prism/; RRID: SCR_002798

Other

Ni+2-NTA Agarose resin	Qiagen	Cat# 30250
ACQUITY UPLC BEH C18 Column, 130Å, 1.7 μm, 1 mm X 100 mm	Waters	Cat# 176000862
ACQUITY UPLC BEH C18 VanGuard Pre-column, 130Å, 1.7 μm, 2.1 mm X 5 mm	Waters	Cat# 186003975
Superdex 200 10/300 GL	GE healthcare	Cat# 28990944
Superdex 200 26/600	GE healthcare	Cat# GE28-9893-36

RESOURCE AVAILABILITY**Lead contact**

Further information and requests for reagents may be directed to, and will be fulfilled by the Lead author, Dr. Anastassios Economou (tassos.economou@kuleuven.be)

Materials availability

This study did not generate new unique reagents.

Data and code availability

MD simulations, smFRET data and HDXMS raw mass spectra files supporting the current study have not been deposited in a public repository because of the large data sizes but are available from the corresponding author on request. Details of PyHDX software for calculation of free energy of exchange from HDXMS data is available in (Smit et al., 2020). The python source code of PyHDX is available in the following Github repository under a standard MIT license, <https://github.com/Jhsmit/PyHDX>. Code for centrality measures and H-bond clustering in proteins along with other MD simulations is available in the following Mendeley data repository: Karathanou (2020) 'Centrality measure and H-bond clustering in proteins' <https://doi.org/10.17632/wbprcvz6h2.2>.

EXPERIMENTAL MODEL AND SUBJECT DETAILS

For protein purification, *E. coli* BL21 (DE3) cells were transformed with plasmids containing the relevant protein derivative gene (Table S6). Cells were grown at 37°C in 5 L flasks (2.5 L; LB) until required OD was reached (OD₆₀₀ 0.6-0.7; 2-3 h). Gene expression was induced with 0.2 mM IPTG and cells were grown for a further 3 h at 30°C. Cells were collected (5000 x g; 4°C; 15 min; Avanti J JLA8.1000 rotor; Beckman Coulter) and subsequently lysed using a French press (8000 psi; 3-5 passes; pre-cooled cylinder at 4°C).

METHOD DETAILS

For list of buffers used, plasmids and mutagenesis see [Supplemental information](#).

Molecular dynamics simulations

We performed atomistic MD simulations of the *E. coli* SecA monomer (*ecSecA*_{2VDA}), and two independent simulations of *ecSecA* dimers. In all simulations, we considered standard protonation for all titratable groups, i.e., Asp and Glu are negatively charged, Arg and Lys, positively charged, and His groups are singly protonated. Simulation systems of the proteins in aqueous solution were prepared using CHARMM-GUI (Jo and Kim, 2008; Jo et al., 2008); ions were added for charge neutrality.

To study the dynamics of the *ecSecA*_{2VDA} monomer we used a coordinate snapshot from the NMR ensemble of SecA structures (Gelis et al., 2007). *E. coli* SecA dimer models with a Wide-open PBD and a closed ATPase motor were generated by threading the structure of the SecA monomer separately onto dimers of *B. subtilis* SecA (PDB ID: 1M6N) and *M. tuberculosis* PDB ID: 1NL3_1, two of the dimeric conformations proposed as physiologically relevant (Gouridis et al., 2013), hereafter *ecSecA*_{1M6N} and *ecSecA*_{1NL3_1}. The simulation systems for the SecA monomer and dimers contain in total 345,330 (*ecSecA*_{2VDA}), 635,979 (*ecSecA*_{1M6N}), and 666,629 atoms (*ecSecA*_{1NL3_1}).

Interactions between atoms of the system were computed using the CHARMM 36 force field (Brooks et al., 1983; MacKerell et al., 1998; MacKerell et al., 2004) with TIP3P water (Jorgensen et al., 1983). All simulations were performed with NAMD (Kalé et al., 1999; Phillips et al., 2005) using a Langevin dynamics scheme (Feller et al., 1995; Martyna et al., 1994). Geometry optimization and an initial 25ps initial equilibration with velocity rescaling were performed with soft harmonic restraints; all harmonic restraints were switched off for the production runs. Equilibration was performed in the *NVT* ensemble (constant number of particles *N*, constant volume *V*, and constant temperature *T*), and all production runs in the *NPT* ensemble (constant pressure *P*) with isotropic pressure coupling. Equilibration and the first 500ps of production runs were performed with an integration step of 1fs and all remaining production runs with a multiple timestep integration scheme using 1fs for bonded forces, 2fs for short-range non-bonded, and 4fs for long-range electrostatics. We used smooth-particle mesh Ewald summation for Coulomb interactions and a switch function between 10 and 12Å for short-range real-space interactions.

H-bond graphs and long-distance conformational coupling

To characterize protein conformational dynamics and identify H-bond paths for long-distance conformational couplings we used algorithms based on graph theory and centrality measures (Karathanou and Bondar, 2019).

Protein groups were considered as H-bonded when the distance between the hydrogen and the acceptor heavy atom, *d*_{HA}, is ≤ 2.5 Å. We computed H bonds between protein sidechains, and between protein sidechains and backbone groups. From each simulation, we derived lists of H-bonded pairs and their interaction distances and constructed adjacency matrices. These are binary matrices representing the H-bond interactions between groups (=1 if there is an H-bond connection between each amino-acid pair in the protein, and 0 otherwise). Adjacency matrices allowed us compute H-bond graphs whose nodes (vertices) are H-bonding residues, and edges, H-bonds.

For simplicity, we visualize H-bond networks by drawing unique lines between C α atoms of pairs of residues that H-bond. These lines are coloured according to the frequency, or occupancy, of H-bonding, defined as the percentage of the analysed trajectory segment during which the two residues are H-bonded.

Using graphs, we monitored nodes and their possible interactions in the network and created clusters, i.e. paths of connected nodes (Karathanou and Bondar, 2018, 2019). To find the shortest H-bonded pathways between SecA protein domains, we use the Dijkstra's algorithm (Cormen et al., 2009). The algorithm starts with an initial (source) and end node and finds the shortest pathway between those nodes based on positive weights. Edge weight is 1 if there is an H-bond connection between each amino-acid pair in

the protein during the simulation time used for analysis and 0 otherwise. A shortest path between two nodes has the least number of intermediate nodes. We obtain the most frequently visited H-bond paths by inverting the H-bond frequencies and setting them as positive weights in Dijkstra's algorithm.

To identify groups important for connectivity within H-bond clusters, we computed the Betweenness Centrality (BC) (Freeman, 1977, 1979) and the Degree Centrality (DC) (Freeman, 1979) of each H-bonding amino acid residue. The BC of node n is given by the number of shortest-distance paths that link any other two nodes ($v1, v2$) and pass via node n , divided by the total number of shortest paths linking $v1$ and $v2$. BC of node n can be normalized by dividing its BC by the number of pairs of nodes in the graph not including n . The DC (Freeman, 1977, 1979) of node n , equals the number of edges connecting to n . DC of node n can be normalized by dividing its DC by the maximum possible edges to n (which is $N-1$, where N is the number of total nodes in the graph). For the H-bond clusters computed here, high BC values indicate H-bonding residues that are part of many H-bond paths, whereas high DC indicates high local H-bond connectivity.

Data analyses scripts were implemented in Tcl within VMD (Humphrey et al., 1996). Additional data processing was performed using MATLAB (Version R2017b, MathWorks). Unless specified otherwise, average values were computed from the last 200 ns of the monomeric and last 100 ns of the dimeric SecA simulations.

Molecular cloning

Genes were cloned in the plasmid vectors listed in Table S5. Mutations were introduced on genes via the QuickChange Site-Directed Mutagenesis protocol (Stratagene-Agilent) using the indicated vector and primers (see Table S5). Restriction enzymes and T4 DNA Ligase were purchased from Promega. For PCR mutagenesis PFU Ultra Polymerase (Stratagene) was used; for gene amplification either Expand High fidelity Polymerase (Roche) or PFU Ultra polymerase (Promega). DpnI was used to cleave the maternal methylated DNA (Promega). Primers (Table S6) were synthesized by Eurogentec (Belgium). All PCR-generated plasmids were sequenced (Macrogen Europe). Plasmids were stored in DH5 α cells.

Protein purification

SecA and derivatives were expressed and purified as described (Gouridis et al., 2013; Papanikolaou et al., 2007). In brief, proteins were overexpressed in BL21 (DE3) cells and purified at 4°C, using home-made Cibacron-Blue resin (Sephacrose™ CL-6B; GE healthcare) followed by two consecutive gel filtration steps (HiLoad 26/600 Superdex 200 pg; GE healthcare), the first in buffer A (50 mM Tris-HCl, pH 8.0, 1M NaCl), the second in buffer B (50 mM Tris-HCl, pH 8.0, 50 mM NaCl), and stored in buffer C (50 mM Tris-HCl, pH 8.0, 50 mM NaCl, 50% v/v glycerol) at -20°C. The His-tagged derivatives of SecA-D2 and proPhoA were purified as previously described (Chatzi et al., 2017; Vandenberk et al., 2019) and stored in buffer C or D (buffer C with 6 M urea) respectively. All proteins were purified to >95% purity, as assessed by gel filtration chromatography and SDS-PAGE.

SecYEG-IMVs and derivatives were prepared as previously described (Lill et al., 1989, 1990) and stored at -80°C. SecY concentration in these preparations was determined as described (Gouridis et al., 2013). All Sec translocase components and preprotein preparations were tested in ATPase and *in vitro* preprotein translocation assays.

Fluorescent labeling of SecA and sample preparation for smFRET and PIE

His-SecA-D2 (10 nmol) in buffer H (50 mM Tris-HCl pH 8.0, 50 mM NaCl, 0.1mM EDTA) was treated with 10 mM DTT (1 h; 4°C), diluted to 1 mL with buffer B and added immediately onto an anion exchange resin (Q resin; GE Healthcare; 0.2 mL; equilibrated in buffer H) and incubated (5 min). The resin was subsequently washed twice with buffer H (2 x 5 mL). Alexa555-maleimide (Thermo Fisher Scientific, 50 nmol) and Alexa647-maleimide (Thermo Fisher Scientific, 50 nmol) were dissolved in 5 μ L DMSO. The dissolved dyes were diluted in 1 mL buffer H and added onto the resin and incubated (under gentle agitation; 12 h; 4°C shielded from light). The resin was washed with 3 mL buffer H to remove excess of dyes and allowed to settle. Proteins were eluted with buffer I (600 μ L; 50 mM Tris-HCl pH 8.0, 1 M NaCl, 0.1mM EDTA). Subsequently, analytical gel filtration (Superdex 200 Increase PC 10/300; GE Healthcare) was carried in buffer J (50 mM Tris-HCl pH 8.0, 50 mM NaCl, 0.01mM EDTA) while recording the absorbance at 280 nm (protein), 555 nm (Alexa555), and 645 nm (Alexa647). The labeling ratio was estimated (>80%) based of the protein absorbance and fluorescent intensities and their corresponding extinction coefficient (ϵ) ($\epsilon_{\text{SecA}} = 75750 \text{ cm}^{-1}\text{M}^{-1}$, $\epsilon_{\text{Alexa555}} = 158000 \text{ cm}^{-1}\text{M}^{-1}$ and $\epsilon_{\text{Alexa647}} = 265000 \text{ cm}^{-1}\text{M}^{-1}$).

To study the monomeric state of SecA and derivatives the concentration of the fluorescently labelled protein was kept at 50-100 pM; the dimeric state was generated upon addition of unlabelled SecA at 0.5-1.0 μ M. Incubation with different partners (ADP, unlabelled SecA, SecYEG embedded in IMVs and signal peptide) was performed at 4°C for 30min.

Single-molecule fluorescence microscopy and PIE

Single-molecule PIE experiments were performed at 20°C using the MicroTime 200 (Picoquant, Germany). Typical average laser powers were 70 μ W at 532 nm and 30 μ W at 640 nm. Fluorescence emitted by diffusing molecules in solution at the focus was collected by the same water objective (UPLSAPO 60x Ultra-Planapochromat, NA 1.2, Olympus), focused onto a 75 μ m pinhole and separated onto two Single-photon avalanche diodes (SPAD) with appropriate spectral filtering (donor channel: 582/64 BrightLine HC (F37-082); acceptor channel: 690/70H Bandpass (F49-691); both AHF Analysentechnik).

PIE data analysis

Analysis was performed as described (de Boer et al., 2019; Ploetz et al., 2016). Briefly, the stoichiometry S and apparent FRET efficiency E^* were calculated for fluorescent bursts having at least 200 photons, to yield a two-dimensional histogram (Kapanidis et al., 2004). Uncorrected FRET efficiency E^* monitors the proximity between the two fluorophores via normalization of sensitized acceptor emission to the total fluorescence of both fluorophores during green excitation. S is defined as the ratio between the overall green fluorescence intensity over the total green and red fluorescence intensity and describes the ratio of donor-to-acceptor fluorophores in the sample.

$$E^* = \frac{F(\text{DA})}{F(\text{DA}) + F(\text{DD})} \quad S = \frac{F(\text{DD}) + F(\text{DA})}{F(\text{DA}) + F(\text{DD}) + F(\text{AA})}$$

We used published procedures to identify bursts corresponding to single molecules (Eggeling et al., 2001). For this we used three parameters characterizing the burst: total of L photons with M neighbouring photons within a time interval of T microseconds. For the data presented in this study, a dual-colour burst search (Nir et al., 2006), using parameters $M = 35$, $T = 500 \mu\text{s}$ and $L = 50$, was applied. Additional thresholding removed spurious changes in fluorescence intensity and selected for intense single-molecule bursts (all photons > 200 photons unless otherwise mentioned). E^* and S values for each burst and thus for individual molecules were binned into a two-dimensional histogram, where we selected donor-acceptor-containing sub-populations according to their intermediate S values. The one-dimensional E^* histograms were fitted with a mixture model of a variable number of Gaussian distributions (1-3). In the fitting procedure the mean and the amplitude were derived from fitting, whereas the standard deviation was fixed or allowed to vary over a small region defined from static DNA samples having attached fluorophores at specific positions (Figure S3). We used the minimum number of distributions that fitted the experimental data, in which the mean value defines the apparent FRET value (E^*) and the amplitude the abundance of a conformational state.

Confocal scanning microscopy and data analysis

To gain information on possible conformational sampling of SecA at room temperature, we used the same home-built confocal microscope as described before (Gouridis et al., 2015). Surface scanning was performed using a XYZ-piezo stage with $100 \times 100 \times 20 \mu\text{m}$ range (P-517-3CD with E-725.3CDA, Physik Instrumente). The detector signal was registered using a Hydra Harp 400 picosecond event timer and a module for time-correlated single photon counting (both Picoquant). The data, e.g., time traces and scanning images, were extracted using ALEX suite custom software. Data were recorded with constant 532-nm excitation at an intensity of $0.5 \mu\text{W}$. Surface immobilization was conducted using an anti-His antibody and established surface-chemistry protocols as described (Gouridis et al., 2015).

Amide hydrogen/deuterium exchange mass spectrometry

HDX sample preparation: SecA and derivatives (see Supplementary material) were dialyzed overnight into buffer E (50 mM Tris-HCl pH 8.0, 50 mM KCl, 1 mM MgCl_2 , 1 mM DTT) and concentrated ($\sim 100 \mu\text{M}$) using centrifugal filters (Vivaspin 500, Sartorius). In the *apo* condition, the protein stock was diluted into aqueous buffer B at 1:5 ratio prior to dilution in D_2O . For the ADP-bound state, SecA was incubated with 20 mM nucleotide, prior to dilution into D_2O (2 mM final nucleotide concentration in D exchange reaction). To monitor SecA:proPhoA₁₋₁₂₂ interactions, proPhoA₁₋₁₂₂ (in Buffer D) was diluted in buffer E to a final concentration of 250 μM (0.2 M Urea), immediately added to SecA at 1:10 ratio (SecA: proPhoA₁₋₁₂₂) and incubated for 2 minutes prior to D exchange. For the SecA:SecYEG state, IMVs were sonicated as described (Chatzi et al., 2017; Gouridis et al., 2010) and incubated with SecA at 1:1.5 (SecA:SecY) molar ratio, for 2 min on ice, prior to D exchange. All mutant proteins were handled similar to the wild type ones and reactions were maintained at similar molar ratios.

D exchange reaction: Isotope labeling was carried out using lyophilized buffer F (50 mM Tris-HCl pH 8.0, 50 mM KCl, 1 mM MgCl_2 , 4 μM ZnSO_4) reconstituted in 99.9% D_2O (Euriso-top), with fresh TCEP [tris(2-carboxyethyl)phosphine] added at 2 mM. Buffer pH_{read} was adjusted to 8.0 using NaOD (Sigma). D exchange buffer was pre-incubated in a 30°C water bath, and the D exchange reaction was initiated by diluting 200 pmol of protein into D_2O buffer F at a 1:10 ratio (final D_2O concentration 90%). Final concentration of SecA was maintained at 4 μM in the D exchange reaction. Continuous labeling reaction was incubated for various time points (10 s, 30 s, 1 min, 2 min, 5 min, 10 min, 30 min and 48 h), primarily at 30°C . For D exchange experiments carried out at 18°C , fewer time points were obtained (1 min, 5 min, 10 min, 30 min, 60 min).

Quenching: The D exchange reaction was quenched by the addition of pre-chilled quench buffer G (1.3% formic acid, 4 mM TCEP, 1 mg/mL fungal protease XIII) at a 1:1 ratio (final pH of 2.5), and incubated (4°C ; 2 min). In samples containing SecYEG IMVs, the reaction was centrifuged at $20000 \times g$ for 90 s on a benchtop cooled centrifuge (Eppendorf), the supernatant containing SecA peptides was collected and immediately injected into the LC-MS system. 100 pmol of SecA was injected into a nanoACQUITY UPLC System with HDX technology (Waters, UK) coupled to a SYNAPT G2 ESI-Q-TOF mass spectrometer. For enhanced peptide coverage, SecA was digested in 2 steps, first with fungal protease XIII (Sigma) (Wowor et al., 2014) at the quench step, and subsequently online digestion on a home-packed immobilized pepsin (Sigma) cartridge (2 mm x 2 cm, Idex), at 16°C . The resulting peptides were loaded and trapped onto a VanGuard C18 Pre-column, (130 \AA , 1.7 mm, 2.1 x 5 mm, Waters) at $100 \mu\text{L}/\text{min}$ for 3 min using 0.23% (v/v) formic acid. Peptides were subsequently separated on a C18 analytical column (130 \AA ,

1.7 mm, 1 x 100 mm, Waters) at 40 mL/min. UPLC separation (solvent A: 0.23% v/v formic acid, solvent B: 0.23% v/v formic acid in acetonitrile) was carried out using a 12 min linear gradient (5-50% solvent B). At the end, solvent B was raised to 90% for 1 min for column cleaning. Peptide trapping-desalting and separation were performed at 2°C. The MS parameters were as follows: capillary voltage 3.0 kV, sampling cone voltage 20 V, extraction cone voltage 3.6 V, source temperature 80°C, desolvation gas flow 500 L/h at 150°C. Full deuteration controls were obtained by incubating SecA in buffer F containing 6M Urea-d4 (98% D, Sigma) overnight at room temperature. D-uptake (%) was calculated using the full deuteration control D-uptake values. Deuterium/Protium back exchange values for our instrumental set up was calculated to be between 20-45% depending on peptide composition. These values are consistent with previously reported studies using similar instrumental set ups (Walters et al., 2012). The data has not been corrected for back exchange and is represented either as absolute D values or as a percent of the full deuteration control (Wales et al., 2013).

Peptide identification and HDX data analysis

Peptide identification was carried out using 100 pmol of protein diluted in protiated buffer F. The sample was quenched as described above and analysed in the MS^F acquisition mode in a nanoACQUITY UPLC System with HDX technology (Waters, UK) coupled to a SYNAPT G2 ESI-Q-TOF mass spectrometer over the m/z range 100-2,000 Da. The collision energy was ramped from 15 to 35 V. Other instrument parameters were as described above. Peptide identification was performed using ProteinLynx Global Server (PLGS v3.0.1, Waters, UK) using the primary sequence of SecA or derivatives as a search template. Peptides were individually assessed for accurate identification and were only considered if they had a signal to noise ratio above 10 and a PLGS score above 7.5. Further, peptides were only considered if they appeared in 3 out of 5 replicate runs for each protein. Data analysis was carried out using DynamX 3.0 (Waters, Milford MA) software to compile and process raw mass spectral data and generate centroid values to calculate relative deuteration values.

Binding of MANT-ADP to the SecA subunit of the translocase

Binding of MANT-ADP to the ATPase motor of SecA results in a strong increase in fluorescence intensity due to the hydrophobic environment within the nucleotide binding cleft (Galletto et al., 2000). Fluorescence intensity was measured on a Cary Eclipse fluorimeter (Agilent) at fixed wavelengths $\lambda_{\text{ex}} = 356$ nm and $\lambda_{\text{em}} = 450$ nm. Excitation slit was at 2.5 nm and emission slit was at 5 nm. All experiments were carried out in 1 mL of buffer K (50 mM Tris-HCl pH 8, 50 mM NaCl, 1 mM MgCl₂). MANT-ADP was maintained at 1 μ M. 1 μ M of SecA/SecYEG:SecA was added at t=30 sec and fluorescence intensity was monitored for 5 min. In ADP chase experiments, 2 mM of cold ADP was added at t= 90 sec and fluorescence was monitored till t= 5 min. Data are presented as an average of 3 replicate measurements. Fluorescent measurement graphs were smoothed using cubic spline smoothing (GraphPad Prism 5).

Miscellaneous

Structural analysis was performed and movies were generated using Pymol (<https://pymol.org/>) and sequence conservation was visualized onto the structure using ConSurf (Ben Chorin et al., 2020). Affinity determination of SecA and/or proPhoA for the translocase, SecA ATPase activity, *in vivo* proPhoA and PhoA translocation, *in vitro* proPhoA translocation, SecA activation energy determination, *in vivo* SecA complementation were as described (Chatzi et al., 2011; Gouridis et al., 2009, 2010, 2013).

QUANTIFICATION AND STATISTICAL ANALYSIS

Quantification and statistical analysis for FRET data

Statistical analysis was performed with Origin software version 2018 (OriginLab), Matlab R2014b (MathWorks). FRET histograms were fitted with a Gaussian mixture model with a restricted standard deviation (see [method details](#) section for details). The data (means and the amplitudes) correspond to mean of 3-5 repeated experiments (i.e. independent protein purification and labelled sample).

HDX-MS data interpretation and visualization

D exchange experiments were carried out in technical triplicates for most conditions (details in [Table S3](#)), and experiments were performed over multiple days to control for day-to-day instrument variation. Further, SecA apo data were obtained from 3 separate protein purifications (biological triplicates) and data was compared to check for any biological or technical variability. All spectra were individually inspected and manually curated to ensure accurate centroid calculations. Maximum errors between replicate runs were found to be ± 0.15 Da with most errors within ± 0.08 Da, thus a difference of ± 0.5 Da between peptides from different states was considered significant (Houde et al., 2011). Comparison between different states of SecA was carried out by considering one state as the control and the other as the test state. D-uptake values were first converted to %D values (as a percentage of 100% deuteration control). %D values of the control state were subtracted from the test state. Positive values indicated increased dynamics and negative values indicated decreased dynamics in the test state compared to the control state. Comparison between states was carried out only on the same peptide and time point obtained from different states. A significant difference in D-uptake in a peptide between two states was identified if it satisfied 2 criteria: a. $> \pm 0.5$ Da absolute difference in deuterium exchange (Houde et al., 2011),

and b. >10% difference in % D values between the 2 states. A peptide was considered different in dynamics if 1 or more time points showed significant differences in D-uptake between 2 compared states. Differences observed within 5 min of D exchange were weighted with greater importance as these time points are hypothesized to monitor the determinants of sub-second domain motions (as determined by smFRET). The peptides that showed significant differences were further classified into those with minor and major differences based on difference in % exchange between the two states; differences between 10%-20% were considered minor and differences > 20% were considered major changes.